The European Space Agency BIOMASS mission: Measuring forest above-ground biomass from space

The European Space Agency BIOMASS mission: measuring forest above-ground biomass from space

Shaun Quegan[1], Thuy Le Toan[2], Jerome Chave[3], Jorgen Dall[4], Jean-François Exbrayat[5], Dinh Ho Tong Minh[6], Mark Lomas[1], Mauro Mariotti D'Alessandro[7], Philippe Paillou[8], Kostas Papathanassiou[9], Fabio Rocca[7], Sassan Saatchi[10], Klaus Scipal[11], Hank Shugart[12], T. Luke Smallman[5], Maciej J. Soja[13], Stefano Tebaldini[7], Lars Ulander[14], Ludovic Villard[2] and Mathew Williams[5]

1. University of Sheffield and National Centre for Earth Observation, UK
2. Centre d'Etudes Spatiales de la Biosphère, CNRS-CNES-Université Paul Sabatier-IRD, Toulouse, France
3. Université Toulouse III Paul Sabatier, Laboratoire Evolution & Diversité Biologique, Toulouse, France
4. Technical University of Denmark, National Space Institute, Denmark
5. University of Edinburgh, School of GeoSciences and National Centre for Earth Observation, UK
6. UMR TETIS, IRSTEA, University of Montpellier, 34093 Montpellier, France
7. Dipartimento di Elettronica Informazione e Bioingegneria, Politecnico di Milano, Italy
8. Université de Bordeaux, Pessac Cedex, France
9. German Aerospace Center e.V. (DLR), Wessling, Germany
10. Jet Propulsion Laboratory, Pasadena, USA10. Mission Science Division, ESA-ESTEC, the Netherlands
11. Mission Science Division, ESA-ESTEC, the Netherlands
12. University of Virginia, Charlottesville, Virginia USA
13. MJ Soja Consulting, Hobart, Tasmania, Australia and University of Tasmania, Hobart, Tasmania , Australia
14. Chalmers University of Technology, Sweden

Corresponding author

Shaun Quegan

School of Mathematics and Statistics

Hicks Building, University of Sheffield,

Hounsfield Rd

Sheffield S3 7RH

UK

Tel: +44 114 2223778 Fax: + 44 114 2223809

Email: s.quegan@sheffield.ac.uk

Abstract

The primary objective of the European Space Agency's 7th Earth Explorer mission, BIOMASS, is to determine the worldwide distribution of forest above-ground biomass (AGB) in order to reduce the major uncertainties in calculations of carbon stocks and fluxes associated with the terrestrial biosphere, including carbon fluxes associated with Land Use Change, forest degradation and forest regrowth. To meet this objective it will carry, for the first time in space, a fully polarimetric P-band synthetic aperture radar (SAR). Three main products will be provided: global maps of both AGB and forest height, with a spatial resolution of 200 m, and maps of severe forest disturbance at 50 m resolution (where "global" is to be understood as subject to Space Object tracking radar restrictions). After launch in 2022, there will be a 3-month commissioning phase, followed by a 14-month phase during which there will be global coverage by SAR tomography. In the succeeding interferometric phase, global polarimetric interferometry Pol-InSAR coverage will be achieved every 7 months up to the end of the 5-year mission. Both Pol-InSAR and TomoSAR will be used to eliminate scattering from the ground (both direct and double bounce backscatter) in forests. In dense tropical forests AGB can then be estimated from the remaining volume scattering using non-linear inversion of a backscattering model. Airborne campaigns in the tropics also indicate that AGB is highly correlated with the backscatter from around 30 m above the ground, as measured by tomography. In contrast, double bounce scattering appears to carry important information about the AGB of boreal forests, so ground cancellation may not be appropriate and the best approach for such forests remains to be finalized. Several methods to exploit these new data in carbon cycle calculations have already been demonstrated. In addition, major mutual gains will be made by combining BIOMASS data with data from other missions that will measure forest biomass, structure, height and change, including the NASA Global Ecosystem Dynamics Investigation lidar deployed on the International Space Station after its launch in December 2018, and the NASA-ISRO NISAR L- and S-band SAR, due for launch in 2022. More generally, space-based measurements of biomass are a core component of a carbon cycle observation and modelling strategy developed by the Group on Earth Observations. Secondary objectives of the mission include imaging of sub-surface geological structures in arid environments, generation of a true Digital Terrain Model without biases caused by forest cover, and measurement of glacier and icesheet velocities. In addition, the operations

67 needed for ionospheric correction of the data will allow very sensitive estimates of ionospheric Total
68 Electron Content and its changes along the dawn-dusk orbit of the mission.

69

70 **1. Introduction: The role of biomass in the global carbon cycle and climate**

71 For millennia, humanity has depended on woody biomass from forests as a source of materials and
72 energy (Rackham and Moody, 1996; Radkau, 2012), and this dependence shows no sign of abating. For
73 example, around a third of the world's population relies on biomass for energy, and in sub-Saharan
74 Africa around 81% of the energy use by households is provided by burning woody biomass (World
75 Bank, 2011). At the same time, forest, and its associated biomass, has often been treated as an
76 impediment to development, and huge tracts have been cleared, and continue to be cleared, to make
77 way for agriculture, pasture and agro-forestry (FAO, 2016). However, a significant shift in the
78 relationship between mankind and biomass has occurred as climate change has become of pressing
79 international concern and the role of forest biomass within this process has become clearer (IPCC, 2007,
80 2013).

81 Climate change is intimately connected with the global carbon balance and the fluxes of greenhouses
82 gases, especially carbon dioxide (CO_2), between the Earth's surface and the atmosphere
83 (Intergovernmental Panel on Climate Change (IPCC), 2007, 2013). In particular, an unequivocal
84 indication of man's effect on our planet is the accelerating growth of atmospheric CO_2. The principal
85 contribution (around 88%) to this growth is emissions from fossil fuel burning, with most of the
86 remainder arising from Land Use Change in the tropics (Le Quéré, 2018). However, the increase in the
87 concentration of atmospheric CO_2 between 2007 and 2016 is only about half (44%) of the emissions.
88 Because CO_2 is chemically inert in the atmosphere, the "missing" half of the emissions must flow back
89 into the Earth's surface. Current estimates (Le Quéré et al., 2018) suggest that around 28% of the total
90 emissions are taken up by the land and 22% by the oceans (leaving around 6% unaccounted for), but
91 there are large uncertainties in these values, especially the land uptake, whose value has usually been
92 estimated as a residual that ensures the total amount of carbon is conserved, as expressed in eq. (1):

93 $$U_{land} = E_{ff} + E_{lb} - (\Delta C_{atmos} + U_{ocean}) . \quad (1)$$

Here E_{ff} denotes fossil fuel emissions; E_{lb} is net land biospheric emissions, comprising both Land Use Change and ecosystem dynamics, and including alterations to biomass stocks linked to process responses to climate change, nitrogen deposition and rising atmospheric CO_2; ΔC_{atmos} is the change in atmospheric CO_2; and U_{land} and U_{ocean} are net average uptake by the land and ocean respectively. In eq. (1) the quantities on the right-hand side are typically estimated on an annual basis or as a decadal average, using a mixture of measurements and models, to yield U_{land}. However, in Le Quéré et al. (2018) U_{land} is estimated independently using dynamic global vegetation models. Under both approaches U_{land} has the largest uncertainty of any term in eq. (1), estimated as 0.8 GtC/yr, which is 26% of its estimated value of 3.0 GtC/yr (1 GtC = 10^9 t of C which is equivalent to 3.67×10^9 t of CO_2). Moreover, the Land Use Change flux (which is the difference between emissions from forest loss and uptake of CO_2 by forest regrowth) has an uncertainty of 0.7 GtC/yr, which is 54% of its estimated value of 1.3 GtC/yr. Since the fractional carbon content of dry biomass is around 50% (though with significant inter-species differences [Thomas and Martin, 2012]), biomass change is a fundamental component in these two land fluxes, controlling the emissions from forest disturbance and the uptake of carbon by forest growth (e.g. Pan et al. 2011). This is why above-ground biomass (AGB) is recognised as an Essential Climate Variable (ECV) within the Global Climate Observing System (2015, 2017).

Climate change concerns have therefore made it imperative to obtain accurate estimates of biomass and its changes. Unfortunately, where this information is most needed – the tropics – is where almost no data have been gathered (Schimel et al., 2015). This is in contrast to forests in the temperate and southern parts of the boreal zones whose economic importance has driven the development of extensive national inventories (although there are vast areas of Alaska, Northern Canada, and East Eurasia that do not have forest inventories because of their low economic importance). The tropical forests cover an enormous area (~18 million km^2) and offer huge logistical challenges for ground-based biomass inventory. They are also crucial in political efforts to mitigate climate change. In particular, the United Nations Convention on Climate Change (UNFCCC) through its Reduction of Emissions from Deforestation and Degradation (REDD+) initiative (UNFCCC, 2016) aims to use market and financial incentives to

transfer funds from the developed world to the developing countries in the tropical belt to help them reduce emissions by preservation and management of their forests (UN-REDD Programme, 2008).

Estimates of biomass losses have focused on deforestation, i.e. conversion of forest land to other land use, which results in complete removal of AGB. However, also significant, but missing from most current estimates, is forest degradation. This is the loss of part of biomass, for instance removal of large stems for timber or of understorey plants for replacement by cocoa, or through increased fire along forest edges.

UN-REDD and related programmes have given significant impetus to the acquisition of more *in situ* data in developing countries and this adds to the information available in the periodic reports of the United Nations (UN) Food and Agriculture Organisation (FAO) (FAO 2006, 2010, 2016). However national data in many cases have large gaps, sampling biases, inconsistency of methods, lack spatially explicit information and contain unrepresentative samples, particularly in developing countries. As a result, major efforts have been made to formulate more consistent global approaches that combine forest inventory and satellite data to estimate AGB. Such endeavours have been greatly hampered by the fact that, up until the launch of the Global Ecosystem Dynamics Investigation (GEDI) instrument (see below), there has never been any spaceborne sensor designed to measure biomass, so space-based estimates of biomass have relied on opportunistic methods applied to non-optimal sensors, with the limitations this implies.

In the tropics, the most significant developments have been based on forest height estimates derived from the Geoscience Laser Altimeter System (GLAS) onboard the Ice, Cloud and land Elevation Satellite (ICESat) before its failure in 2009 (Lefsky, 2005, 2010). Combining GLAS data with other EO and environmental datasets and *in situ* biomass measurements has led to the production of two pan-tropical biomass maps (Saatchi et al. 2010; Baccini et al. 2012) at grid scales of 1 km and 500 m respectively; differences between these maps and differences between the maps and *in situ* data are discussed in Mitchard et al. (2013, 2014). Refinements of these maps have been produced by Avitabile et al. (2016) and Baccini et al. (2017) based on essentially the same satellite datasets.

For boreal and temperate forests, methods have been developed to estimate Growing Stock Volume (GSV, defined as the volume of wood in all living trees in an area with diameter at breast height above a given threshold) from very long time series of C-band Envisat satellite radar data (Santoro et al. 2011). Multiplying these GSV estimates by wood density allowed Thurner et al. (2014) to estimate the carbon stock of forests north of 30°N. Reliable GSV estimates using these methods are only possible at spatial resolutions much coarser than the underlying radar data: by averaging to 0.5°, the relative RMS difference between estimated GSV and reference data was consistently found to lie in the range 20–30% (Santoro et al. 2013). Further refinements to the methodology and its combination with ALOS PALSAR-2 data are given in the Final Report of the ESA GlobBiomass project (Schmullius et al., 2017).

L-band radar offers access to biomass values up to around 100 t/ha before losing sensitivity (e.g. Mitchard et al., 2009). Under the JAXA Kyoto and Carbon Initiative, the ALOS L-band PALSAR-1 acquired a systematic five-year archive of forest data before its failure in April 2011 (Rosenqvist et al., 2014). PALSAR-2 launched in spring 2014 and has continued this systematic acquisition strategy, but current JAXA data policy makes scene data very expensive. Annual mosaics are freely available and have been used to map woodland savanna biomass at continental scale (Bouvet et al., 2018), but the mosaics combine data from different times and environmental conditions, so further processing may be needed to exploit them for biomass estimation (Schmullius et al., 2017). L-band data will also be acquired by the two Argentinian Microwave Observation Satellites (SAOCOM), the first of which was launched on October 8, 2018, with the second due in 2019. Their main objectives are measurements of soil moisture and monitoring of hazards, such as oil spills and floods, and their value for global forest observations is not yet clear.

C-band (Sentinel-1, Radarsat) and X-band (Tandem-X) radar instruments are in orbit but at these frequencies most of the backscatter is from the leaves and small twigs, so they have limited value for biomass estimation except within the context of long time series at C-band (Santoro et al. 2011) and, for TanDEM-X, when a ground Digital Terrain Model (DTM) is available and the height-to-biomass allometry is robust (Persson et al., 2017; Askne et al., 2017).

An exciting new development is the deployment on the International Space Station of the NASA GEDI lidar instrument after its launch on December 5, 2018 (see Section 10). This mission aims to sample forest vertical structure across all forests between 51.5° S and 51.5° N, from which estimates of the mean and variance of AGB on a 1 km grid will be derived. In addition, ICESat-2 launched on September 15, 2018; although it is optimised for icesheet, cloud and aerosol applications, and uses a different technical approach from ICESat-1 based on photon counting, preliminary results suggest that it can provide information on both forest height and structure.

It is against this scientific and observational background that BIOMASS was selected by the European Space Agency (ESA) in 2013 as its 7th Earth Explorer mission, and the satellite is now under production by a consortium led by Airbus UK for launch in 2022. The initial mission concept is described in Le Toan et al. (2011), but there have been major developments since that time in almost all aspects of the mission: the measurement and calibration concepts, the scientific context, the methods to recover biomass from the satellite data, the exploitation of biomass in carbon cycle and climate modelling, the availability of P-band airborne campaign data and high quality *in situ* data, and the overall capability to estimate biomass from space. It is therefore timely to provide a comprehensive description of the current mission concept, and this paper sets out to do so.

After a review of the mission objectives (Section 2), the associated measurement techniques (polarimetry, polarimetric interferometry [Pol-InSAR] and SAR tomography [TomoSAR]) are described in Section 3. Pol-InSAR and TomoSAR require the combination of multi-temporal stacks of data; this imposes very strong conditions on the BIOMASS orbit pattern, with significant consequences for the production of global biomass products (Section 4). The orbit pattern also imposes strong requirements on the ability of the AGB and height inversion techniques, discussed in Section 5, to adapt to changing environmental conditions. Section 6 deals with the use of BIOMASS data to estimate severe forest disturbance, while Section 7 describes the development of the reference datasets to be used for algorithm calibration and product validation. In Section 8 we discuss developments in how BIOMASS data can be used to estimate key carbon cycle and climate variables. Section 9 addresses a range of secondary objectives. Section 10 provides a view on how BIOMASS complements other upcoming

missions devoted to forest structure and biomass, in particular the GEDI lidar and the NASA-ISRO NISAR L- and S-band mission. Finally, Section 11 discusses how BIOMASS will contribute to an overall system for measuring biomass and its changes in the context of a global carbon cycle management scheme and presents our general conclusions.

2. BIOMASS mission objectives and data properties

The primary objective of the BIOMASS mission is to determine the worldwide distribution of forest above-ground biomass (AGB) in order to reduce the major uncertainties in calculations of carbon stocks and fluxes associated with the terrestrial biosphere, including carbon fluxes associated with Land Use Change, forest degradation and forest regrowth. In doing so, it will provide support for international agreements such as REDD+ and UN Sustainable Development Goals (#13: climate action; #15: life on land). In addition it has several secondary objectives, including mapping sub-surface geology, measuring terrain topography under dense vegetation and estimating glacier and icesheet velocities (ESA, 2012).

Although BIOMASS aims at full global coverage, it will at least cover forested areas between 75° N and 56° S, subject to US Department of Defense Space Object Tracking Radar (SOTR) restrictions. These restrictions do not currently allow BIOMASS to operate within line-of-sight of the SOTR radars and mainly exclude the North American continent and Europe (Fig. 1, reproduced from Carreiras et al., 2017). For secondary applications, if global coverage is not possible, data will be collected on a best effort basis after covering the primary objectives, with priorities defined as in ESA (2015).

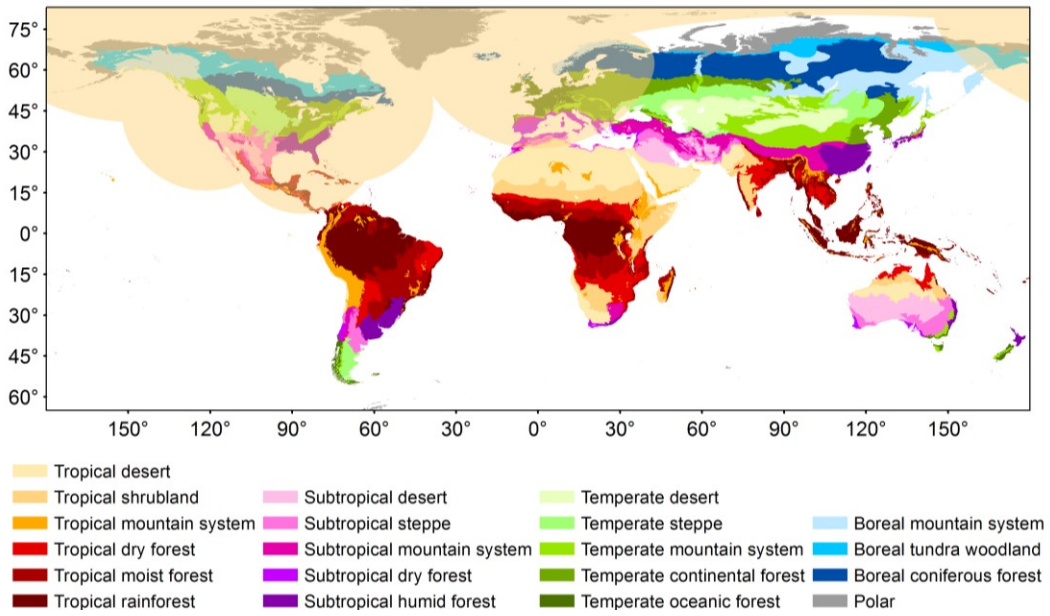

Fig. 1. Global ecological regions of the world (FAO 2012) with the area affected by Space Objects Tracking Radar (SOTR) stations highlighted in yellow. Only land areas between 65° South and 85° North are represented (figure reproduced courtesy of Joao Carreiras).

The BIOMASS data product requirements to meet the primary mission objectives are (ESA, 2015):

1. Above-ground forest biomass (AGB), defined as the dry weight of live organic matter above the soil, including stem, stump, branches, bark, seeds and foliage woody matter per unit area, expressed in t ha^{-1} (FAO, 2009). It does not include dead mass, litter and below-ground biomass. Biomass maps will be produced with a grid-size of 200m x 200m (4 ha).
2. Forest height, defined as upper canopy height according to the H100 standard used in forestry expressed in m, mapped using the same 4 ha grid as for biomass. H100 is defined as the average height of the 100 tallest trees/ha (Philip, 1994).
3. Severe disturbance, defined as an area where an intact patch of forest has been cleared, expressed as a binary classification of intact vs deforested or logged areas, with detection of forest loss being fixed at a given level of statistical significance.

Further properties of these products are defined in Table 1. Note that:

- The biomass and height products will be produced on a 4 ha grid, while the disturbance product is at the full resolution of the instrument after averaging to 6 looks in azimuth, i.e., around 50 m x 50 m. This is because the large changes in backscatter associated with forest clearance mean that disturbance can be detected using less precise estimates of the polarimetric covariance and coherence matrices than are needed for biomass and height estimation.
- If the true AGB exceeds 50 t ha^{-1} then the RMS error (RMSE) of its estimate is expected to depend on biomass and be less than AGB/5. For all values of AGB < 50 t ha^{-1} the RMSE is stipulated to be 10 t ha^{-1} or better, though it is likely that changes in ground conditions, such as soil moisture, may cause the RMSE to increase beyond this value**.** Similarly, the RMSE of estimates of forest height should be less than 30% of the true forest height for trees higher than 10 m**.**
- Below-ground biomass cannot be measured by BIOMASS (or any other remote sensing instrument), but can be inferred from above-ground biomass using allometric relations combined with climate data (Cairn et al., 1997; Mokany et al., 2006; Thurner et al., 2014). In particular, Ledo et al. (2018) used an extensive tropical, temperate and boreal forest dataset to develop a regression, with just tree size and mean water deficit as predictor variables, which explains 62% of the variance in the root-to-shoot ratio. Therefore, throughout this paper, 'biomass' denotes 'above-ground biomass'.

Table 1 Summary of primary BIOMASS Level 2 products. Achieving global coverage requires 425 days during the initial Tomographic Phase and 228 days for each cycle of the subsequent Interferometric Phase. RMSE indicates Root Mean Square Error. "Global" is to be understood as subject to Space Object Tracking Radar restrictions (Carreiras et al., 2017).

Level 2 Product	**Definition**	**Information Requirements**
Forest biomass	Above-ground biomass expressed in t ha^{-1}.	• 200 m resolution

		• RMSE of 20% or 10 t ha^{-1} for biomass < 50 t ha^{-1} • 1 biomass map every observation cycle • global coverage of forested areas
Forest height	Upper canopy height defined according to the H100 standard	• 200 m resolution • accuracy required is biome-dependent, but RMSE should be better than 30% for trees higher than 10 m • 1 height map every observation cycle • global coverage of forested areas
Severe disturbance	Map product showing areas of forest clearance	• 50 m resolution • detection at a specified level of significance • 1 map every observation cycle • global coverage of forested areas

3. The BIOMASS system and measurement techniques

BIOMASS will be a fully polarimetric SAR mission operating at P-band (centre frequency 435 MHz) with 6 MHz bandwidth, as permitted by the International Telecommunications Union under a secondary allocation (the primary allocation is to the SOTR system). The choice of P-band is mandatory for measuring biomass with a single radar satellite (necessary for affordability within the ESA cost envelope) for three main reasons (ESA, 2008, 2012; Le Toan et al., 2011):

1. P-band radiation can penetrate the canopy in all forest biomes and interacts preferentially with the large woody vegetation elements in which most of the biomass resides;
2. Backscatter at P-band is more sensitive to biomass than at higher frequencies (X-, C-, S- and L-bands); lower frequencies (e.g. VHF) display even greater sensitivity (Fransson et al., 2000) but present formidable challenges for spaceborne SAR because of ionospheric effects;

3. P-band displays high temporal coherence between passes separated by several weeks, even in dense forest (Ho Tong Minh et al., 2012), allowing the use of Pol-InSAR to estimate forest height and retrieval of forest vertical structure using tomography.

Here (1) is the crucial physical condition: it underlies the sensitivity in point (2) and, through the relative positional stability of the large woody elements, combined with the greater phase tolerance at longer wavelengths, permits the long-term coherence needed for (3).

The satellite will carry a 12 m diameter reflector antenna, yielding a single-look azimuth resolution of ~7.9 m. A polarimetric covariance product will also be generated by averaging 6 looks in azimuth, giving pixels with azimuth resolution ~50 m. Because of the allotted 6 MHz bandwidth, the single-look slant range resolution will be 25 m, equivalent to a ground range resolution of 59.2 m at an incidence angle of 25°. Roll manoeuvres will allow the satellite to successively generate three sub-swaths of width 54.32, 54.41 and 46.06 km, giving a range of incidence angles across the combined swath from 23° to 33.9°. It will be in a sun-synchronous orbit with a near dawn-dusk (06:00 ± 15 min) equatorial crossing time; the Local Time of the Ascending Node (LTAN) will be on the dawn-side, the system will be left-looking and the orbit inclination will be 98°, with the highest latitude in the northern hemisphere attained on the night-side. This orbit is chosen to avoid the severe scintillations that occur in the post-sunset equatorial ionosphere (Rogers et al., 2013). Observations will be made during both the ascending and descending passes.

BIOMASS displays major advances compared to all previous SAR missions in its use of three complementary technologies to provide information on forest properties: polarimetry (PolSAR), Pol-InSAR and TomoSAR. All acquisitions will be fully polarimetric, i.e. the amplitude and phase of the HH, VV, HV & VH channels will be measured (HV indicates horizontal polarization on transmit and vertical polarization on receive, with the other channels being similarly defined). This is in itself an advance, but BIOMASS will also be the first mission to systematically employ the Pol-InSAR technique to measure forest height. Even more innovative is its tomographic capability, which will allow three-dimensional imaging of forests.

297 The Tomographic Phase will immediately follow the initial 3-month Commissioning Phase, and will
298 provide tomographic mapping of all imaged forest areas. Global coverage requires 425 days (~14
299 months) in order to provide 7 passes, each separated by 3 days, for each tomographic acquisition. The
300 remainder of the 5-year mission will be taken up by the Interferometric Phase, during which 3 passes,
301 each separated by 3 days, will be combined in 3-baseline Pol-InSAR. Each cycle of the Interferometric
302 Phase will require 228 days (~7 months) to provide global coverage. Note that these techniques are
303 nested: the data gathered for tomography will yield multiple Pol-InSAR and PolSAR measurements,
304 and each Pol-InSAR image triplet also provides three PolSAR images.

305 Associated with the highly innovative measurement concepts of the mission are completely new
306 challenges in external calibration arising from the orbital pattern needed for the tomographic and Pol-
307 InSAR phases of the mission (Section 4), the strong effects of the ionosphere at P-band, and the lack of
308 pre-existing P-band data except over very limited parts of the globe. Together these create problems
309 that can only be solved by combining infrequent visits to instrumented calibration sites with systematic
310 exploitation of the properties of distributed targets and targets of opportunity. An overall approach to
311 addressing these problems, including ionospheric correction, radiometric and polarimetric calibration,
312 and providing the required geolocation accuracy is described in Quegan et al. (2018).

313 ## 4. The BIOMASS orbit and its implications

314 In the Tomographic Phase, BIOMASS needs to be placed in a very precise repeat orbit in which a given
315 scene is imaged 7 times with 3-day spacing. These acquisitions will be from slightly different positions
316 separated by 15% of the critical baseline (i.e. 0.823 km) at the equator, which is necessary to preserve
317 coherence. In this orbit, it takes 18 days to acquire the 7 images needed for each of the 3 sub-swaths, so
318 that tomography over the full swath (comprising the 3 sub-swaths) occupies a period of 60 days. Once
319 this has been achieved, a drift manœuvre will raise the satellite in altitude and then return it to its
320 nominal altitude of 671.9 km. This allows the Earth to rotate below the satellite, and the next
321 tomographic acquisition period covers a new swath that is adjacent to the previous one. Repeating this
322 sequence 6 + 1/3 times yields global coverage and takes 425 days (the extra third corresponds to
323 coverage in swath 1). The orbit pattern for the Interferometric Phase uses essentially the same concept,

but because only 3 images are needed to form the Pol-InSAR product, imaging a full swath requires only 24 days, and global coverage takes 228 days.

These properties of the BIOMASS orbit pattern, driven by the requirement for global coverage using coherent imaging techniques, have profound implications for biomass retrieval in time and space. Acquisitions in adjacent swaths are separated by 2 months in the Tomographic Phase and by a little less than a month in each cycle of the Interferometric Phase. Hence there are likely to be significant changes in environmental conditions between different swaths that make up the global coverage. In addition, because each cycle of the Interferometric Phase takes 7 months, the acquisitions become steadily more out of phase with annual geophysical cycles, such as the Amazonian and West African inundation cycles. This means that the BIOMASS inversion algorithms have to be sufficiently robust that they are negligibly affected by environmental changes. Incomplete compensation for such changes will manifest themselves as systematic differences between adjacent swaths or repeat swaths gathered in different cycles. As an example, boreal forests freeze during winter and their backscatter significantly decreases, so the winter season will most likely not be useful for biomass estimation.

5. Forest AGB and height estimation techniques

BIOMASS will exploit properties of all three SAR techniques, PolSAR, Pol-InSAR and TomoSAR, to estimate biomass, while both Pol-InSAR and TomoSAR will provide estimates of forest height. However, because BIOMASS will be the first spaceborne P-band SAR, the experimental data needed to support the development and testing of these techniques is based on limited airborne and ground-based measurements. Six major ESA airborne campaigns were carried out (BioSAR-1, -2 and -3 in the boreal zone, and three in tropical ecosystems: TropiSAR in French Guiana, AfriSAR in Gabon and Indrex-2 in Indonesia) using the E-SAR and F-SAR (DLR, Germany) and SETHI (ONERA, France) P-band SARs (see Table 2, which includes the objectives of the campaigns and essential properties of the test-sites). These campaigns have provided the most accurate and complete set of P-band SAR (PolSAR, Pol-InSAR and TomoSAR) and associated *in situ* data currently available over boreal and tropical

351 forests. In addition, long-term continuous P-band tower-based measurements were made in French
352 Guiana (Tropiscat), Ghana (Afriscat) and Sweden (Borealscat) to investigate diurnal and seasonal
353 variations in backscatter and temporal coherence. Earlier P-band datasets from the NASA AirSAR
354 system were also helpful, especially tropical forest data from Costa Rica, to extend the range of tropical
355 biomass values (Saatchi et al., 2011), and NASA was heavily involved in the AfriSAR campaign,
356 providing lidar coverage of the AfriSAR test-sites (Labrière et al., 2018). No specific ESA campaigns
357 were conducted in temperate forests, but substantial amounts of tomographic data are available for such
358 forests from experimental campaigns carried out by DLR.

359 **Table 2** Campaign data used in developing and testing BIOMASS retrieval algorithms.
360

Campaign	**Objectives**	**Test sites**	**Time**	**Forest conditions**
TropiSAR, SETHI (Dubois-Fernandez et al., 2012)	Biomass estimation in tropical forest; temporal stability of coherence	Paracou & Nouragues, French Guiana	Aug. 2009	Tropical rain forest, AGB 300-500 t/ha, lowland and hilly terrain
Indrex-2, E-SAR (Hajnsek et al., 2009a) ; not tomographic	Height retrieval in tropical forest ; measurement of repeat-pass temporal decorrelation	Sungai-Wai & Mawas, Borneo, Indonesia	Nov. 2004	Tropical rain forest. Sungai-Wai: lowland, AGB ≤ 600 t/ha; Mawas: peat swamp, AGB ≤ 200 t/ha
Tropiscat: Ground-based high temporal resolution measurements (Koleck et al., 2012)	Measurement of long-term temporal coherence and temporal variation	Paracou, French Guiana	Aug. 2011 - Dec. 2012	Tropical rain forest, AGB ca. 400 t/ha

	of backscatter in tropical forest			
BioSAR-1, E-SAR (Hajnsek et al., 2008)	Biomass estimation and measurement of multi-month temporal decorrelation	Remningstorp, southern Sweden	Mar. - May 2007	Hemi-boreal forest, low topography, AGB ≤ 300 t/ha
BioSAR-2, E-SAR (Hajnsek et al., 2009b)	Topographic influence on biomass estimation	Krycklan, northern Sweden	Oct. 2008	Boreal forest, hilly, AGB ≤ 300 t/ha
BioSAR-3, E-SAR (Ulander et al., 2011a, b)	Forest change and multi-year coherence relative to BioSAR-1	Remningstorp, southern Sweden	Sept. 2010	Hemi-boreal forest, low topography, AGB ≤ 400 t/ha (more high biomass stands than in BIOSAR-1)
AfriSAR, SETHI and F-SAR	Biomass estimation in tropical forest; temporal stability of coherence	Sites at Lopé, Mondah, Mabounie and Rabi, Gabon	July 2015 (SETHI) Feb. 2016 (F-SAR)	Tropical forest and savannah, AGB from 50 to 500 t/ha
Afriscat: Ground-based high temporal resolution measurements	Measurement of long-term temporal coherence and temporal variation of backscatter in tropical forest	Ankasa, Ghana	July 2015 - July 2016	Tropical forest, low topography, AGB from 100 to 300 t/ha

Borealscat: Ground-based high temporal resolution measurements (Ulander et al., 2018; Monteith and Ulander, 2018)	Time series of backscatter, tomography, coherence and environmental parameters in boreal forest.	Remningstorp, southern Sweden	Dec. 2016, ongoing	Hemi-boreal forest, spruce-dominated stand, low topography, AGB = 250 t/ha

361

362 **5.1 Estimating AGB**

363 Some key findings from these campaigns are illustrated in Fig. 2, where the P-band HV backscatter
364 (given as γ^0 in dB) is plotted against the biomass of reference plots from a boreal site (Remningstorp,
365 Sweden) and two tropical sites (Paracou, French Guiana and La Selva, Costa Rica). The data are not
366 corrected for topographic or soil moisture effects, and the lines correspond to linear regression fits to
367 the log-log form of the data. The sensitivity of backscatter to biomass is clear across the whole range
368 of biomass covered, though with large dispersion in the boreal forest and the high biomass tropical
369 forest in French Guiana. Also clear is that, for a given biomass, the HV backscatter is considerably
370 larger in boreal than tropical forest. This corrects an error in Fig. 2 of Le Toan et al. (2011) where mean
371 backscatter differences between the boreal and tropical data were ascribed to calibration errors and
372 removed by shifting the data. The careful calibration of the datasets shown in Fig. 2 indicates that the
373 difference is real and that different physical and biological factors (such as forest structure) are at play
374 in the different forest types.

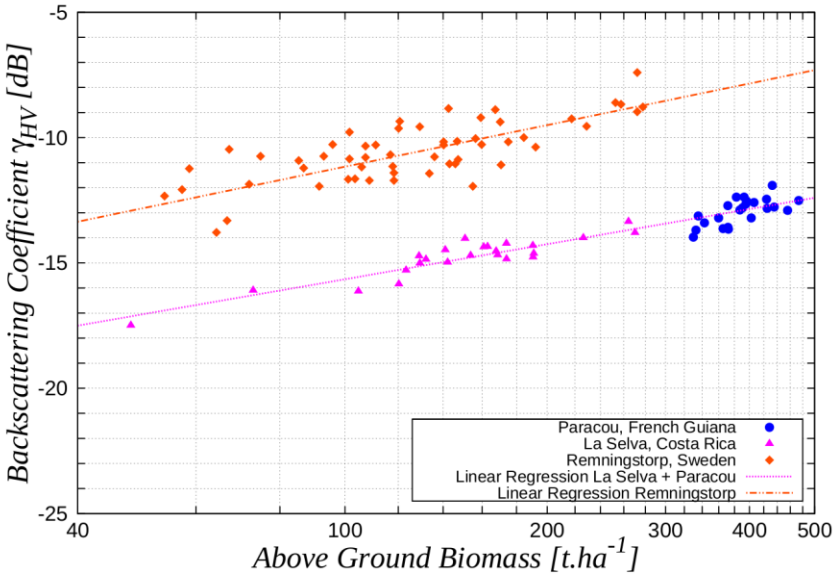

375

376 **Fig. 2.** P-band backscatter at HV polarisation (γ^0_{HV}) over tropical and boreal forests against the biomass
377 of *in situ* reference plots. Data from Paracou, French Guiana, were acquired by the SETHI SAR system
378 in 2011 (Dubois-Fernandez et al., 2012), those from La Selva, Costa Rica, in 2004 by the AIRSAR
379 system (Antonarakis et al., 2011) and those from Remningstorp, Sweden, by the E-SAR system in 2007
380 (Sandberg et al., 2011).

381

382 The regression lines indicate that in natural units the HV backscatter is approximately related to
383 biomass, W, by a power law relationship, i.e.

384 $$\gamma^0_{HV} = cW^p \quad (2)$$

385 where c and p are parameters. Analysis in Schlund et al. (2018) indicates such relationships are found
386 for the full set of available P-band SAR datasets that are supported by adequate *in situ* data except where
387 there is strong topography. Although the model coefficients (and their coefficients of determination)
388 vary across datasets, they are not significantly different when similar AGB ranges are considered.
389 Despite this strong regularity in the relation between HV backscatter and biomass, exploiting it to
390 estimate biomass faces a number of problems:

391 **a. Dispersion in the data**. For the boreal data in Fig. 2, major factors causing dispersion in the
392 backscatter values are slope and soil moisture variations. The Krycklan campaign over boreal forest
393 in Sweden (Table 2) clearly shows that topography severely affects the power law relationship
394 given by eq. (2) (Soja et al., 2013). This is particularly obvious in Krycklan because in this region
395 most of the highest biomass stands are located in sloping areas. As demonstrated in Soja et al.
396 (2013), however, adding terms involving the $\gamma^0_{HH}/\gamma^0_{VV}$ ratio and slope to the regression significantly
397 reduces the dispersion, at the expense of including two extra parameters. Note that the HH/VV ratio
398 was included because of its lower sensitivity to soil moisture, and that the regression inferred from
399 the Krycklan site in N. Sweden could be successfully transferred to Remningstorp 720 km away in
400 S. Sweden. The associated relative RMSEs in AGB using the combined BioSAR-1 and -2 data were
401 27% (35 t/ha) or greater at Krycklan and 22% (40 t/ha) or greater at Remningstorp. However, more
402 recent unpublished analysis including the BIOSAR-3 data indicates that further coefficients are
403 needed to achieve adequate accuracy. Another study for Remningstorp (Sandberg et al., 2014)
404 found that AGB change could be estimated more accurately than AGB itself: analysis based on
405 2007 and 2010 data gave a RMSE of 20 t/ha in the estimated biomass change, i.e. roughly half the
406 RMSEs of the individual AGB estimates. The algorithm used was based on finding areas of little
407 or no change using the HH/VV ratio and applying polarization-dependent correction factors to
408 reduce the effect of moisture variation.
409 Unlike in Sweden, very little environmental change occurred during the TropiSAR campaign in
410 French Guiana, and the major effect affecting the relation given by eq. (2) was topography, which
411 greatly increased the dispersion. Methods to reduce this were based on rotating the spatial axes and
412 normalization to account for the variation in the volume and double bounce backscatter with
413 incidence angle (Villard and Le Toan, 2015). This allowed the sensitivity of the HV backscatter to
414 biomass to be recovered, and AGB could then be estimated from the polarimetric data with relative
415 RMSE < 20%. However, because the approach is based on regression and there was little temporal
416 change in conditions during the campaign, it contains no provision for dealing with large seasonal
417 variations in backscatter like those observed in the Tropiscat data (Bai et al., 2018) and expected in
418 BIOMASS data.

b. **Algorithm training**. Regression methods need training data, but in many parts of the world, and especially in the tropics, there are very few high quality permanent *in situ* sampling plots, almost all funded under science grants. Significant efforts are being made by ESA, in collaboration with NASA, to work with and extend the existing *in situ* networks in order to establish a set of well-documented reference sites that could be using for training and validation. Part of the challenge in doing so is to ensure that the set of reference sites is large enough and representative enough to capture the major variations in forest types and conditions.

c. **Physical explanation**. Despite its remarkable generality, as demonstrated in Schlund et al. (2018), the physical basis of eq. (2) is not well-understood except in certain limiting cases (see below). Hence it is essentially empirical and at present we cannot in general attach meaningful physical properties to the fitting parameters or derive them from scattering models. In particular, it has no clear links to well-known decompositions of polarimetric backscatter into physical mechanisms (e.g. Freeman and Durden (1998); Cloude and Pottier (1996)). In addition, in boreal forests this relation depends on both total AGB and tree number density, so that unambiguous estimates of AGB require information on number density or use of height information combined with height-biomass allometric relations (Smith-Jonforsen et al., 2007)

To get round these problems with the regression-based approaches, the current emphasis is on estimating biomass using a model-based approach that brings together three key factors: the capabilities of the BIOMASS system, the observed properties of the vertical distribution of forest biomass and our knowledge about the physics of radar-canopy interactions as embodied in scattering models.

Its starting point is a simplified scattering model that describes the backscattering coefficient in each of the HH, HV and VV channels as an incoherent sum of volume, surface and double-bounce scattering (Truong-Loï et al., 2015). The model involves 6 real parameters per polarization, which are estimated using a combination of a scattering model and reference data. Biomass, soil roughness and soil moisture are then treated as variables to be estimated from the data. Initial analysis found that this model was too complex and the associated parameter estimation was too unstable for this to be a viable approach for BIOMASS. However, a crucial technical development was to demonstrate that both tomographic and

Pol-InSAR data can be used to cancel out the terms involving the ground (surface scatter and double bounce) and isolate the volume scattering term (Mariotti d'Alessandro et al., 2013; Mariotti d'Alessandro et al., 2018). In the Truong-Loï et al. (2015) formulation, this term can be written as

$$\sigma_{pq}^{v} = A_{pq} W^{\alpha_{pq}} \cos\theta \left(1 - \exp\left(-\frac{B_{pq} W^{\beta_{pq}}}{\cos\theta}\right)\right) \quad (3)$$

where A_{pq}, B_{pq}, α_{pq} and β_{pq} are coefficients for polarization configuration pq, W is AGB, and θ is the local incidence angle. The coefficients α_{pq} and β_{pq} relate to forest structure, $B_{pq} > 0$ is an extinction coefficient and $A_{pq} > 0$ is a scaling factor.

Assuming that A_{pq}, B_{pq}, α_{pq} and β_{pq} are space-invariant at a certain scale, these parameters and AGB can be estimated simultaneously from the measured values of σ_{pq}^{v} in the three polarizations, pq = HH, HV and VV, using a non-linear optimization scheme (Soja et al., 2017, 2018). However, in model (3), the two biomass-dependent factors, $A_{pq} W^{\alpha_{pq}}$ and $1 - \exp\left(-\frac{B_{pq} \mathrm{W}^{\beta_{pq}}}{\cos\theta}\right)$, both increase with increasing AGB for realistic parameters ($\alpha_{pq} > 0$ and $\beta_{pq} > 0$), so interactions between α_{pq}, B_{pq} and β_{pq} render the inversion difficult. This problem can be mitigated by using two special cases of the model, both of which lead to a power law expression as in eq. (2). For the low-attenuation case, i.e., $B_{pq} \mathrm{W}^{\beta_{pq}} \ll 1$, eq. (3) can be simplified using a series expansion to:

$$\sigma_{pq}^{v} = A' W^{p} \quad (4)$$

where $p = \alpha_{pq} + \beta_{pq}$ and $A' = A_{pq} B_{pq}$, and in the high-attenuation case, i.e., $B_{pq} \mathrm{W}^{\beta_{pq}} \gg 1$, eq. (3) can be simplified to:

$$\sigma_{pq}^{v} = A' W^{p} \cos\theta \quad (5)$$

where $p = \alpha_{pq}$ and $A' = A_{pq}$. In both cases, A', W and p can then be estimated using the scheme proposed in Soja et al. (2017, 2018).

Note that there is still an inherent scaling ambiguity since the scheme cannot distinguish the unbiased estimate of AGB, W_0, from any function of the form aW_0^b, where a and b are calibration constants. Hence reference data are needed, but these data do not need to cover a wide range of backscatter, slope and incidence angle conditions, as would be required if any of the models (3) - (5) were to be trained

directly. One complication is that the temporal and spatial variations of a and b are are currently unknown and further work is needed to quantity them. Further refinements may also be needed to reduce residual effects from moisture variations by, for example, use of the VV/HH ratio in boreal forests as discussed above.

The effectiveness of this approach is illustrated by Fig. 3, which plots values of AGB estimated with this scheme against AGB values estimated from *in situ* and airborne laser scanning data for a set of 200 m x 200 m regions of interest (ROIs). The airborne P-band data used are from the AfriSAR campaign and were filtered to 6 MHz to match the BIOMASS bandwidth. The estimates are highly correlated with the reference data (r = 0.97), exhibit only a small amount of bias across the whole biomass range, and give a RMSE of 41 t/ha (16% of the average biomass).

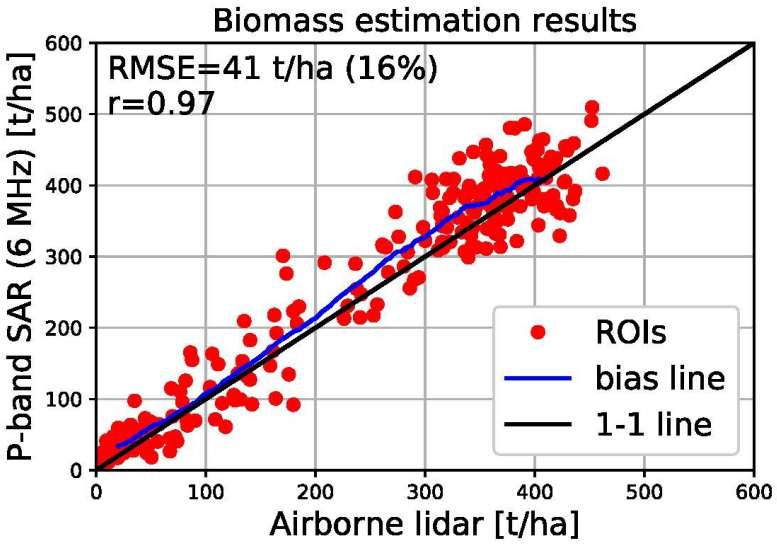

Fig. 3. Estimated AGB using the approach described in the text against AGB estimated from *in situ* and airborne laser scanning at the La Lopé site in Gabon during the AfriSAR campaign. The running average given by the blue line indicates only a small positive bias across the whole range of AGB. ROI denotes Region of Interest.

Further confirmation of the importance of isolating the volume backscatter by using the full power of tomography is from the TropiSAR tropical forest campaign, where the tomographic intensity (in dB) measured at 30 m above the ground (representing scattering from canopy elements between ca. 17.5 m and 42.5 m, given the roughly 25 m vertical resolution of tomographic imaging) was found to be highly

correlated with AGB (Ho Tong Minh et al., 2014, 2016). The observed sensitivity is about 50 tons/ha per dB, and the correlation coefficient is about 0.84 at the scale of 1 ha. This striking result has been replicated in the forest sites investigated during the AfriSAR campaign (Fig. 4), and suggests that the backscatter from the forest layer centred 30 m above ground should be strongly correlated with total AGB in the case of dense tropical forests.

Importantly, this finding is consistent with the TROLL ecological model (Chave, 1999), which predicts that for dense tropical forests the fraction of biomass contained between 20 m and 40 m accounts for about 35% to 40% of the total AGB, and that this relation is stable over a large range of AGB values (Ho Tong Minh et al., 2014). Another element in support of the ecological relevance of the 30 m layer is provided by two recent studies of tropical forests, which observed that: a) correlation between AGB and the area occupied at different heights by large trees (as derived from lidar) is maximal at a height of about 30 m (Meyer et al., 2017); b) about 35% of the total volume tends to be concentrated at approximately 24-40 m above the ground (Tang, 2018).

However, tomographic data will only be available in the first phase of the mission. In addition, exploiting the relation between AGB and the 30 m tomographic layer requires knowledge of how the regression coefficients vary in time and space, hence substantial amounts of training data. In contrast, ground cancellation can be carried out with both tomographic and Pol-InSAR data (so throughout the mission). This allows the volume scattering term (eq. (3)) to be isolated and hence AGB to be estimated using the scheme described in Soja et al. (2018), which makes much less demand on the availability of reference data.

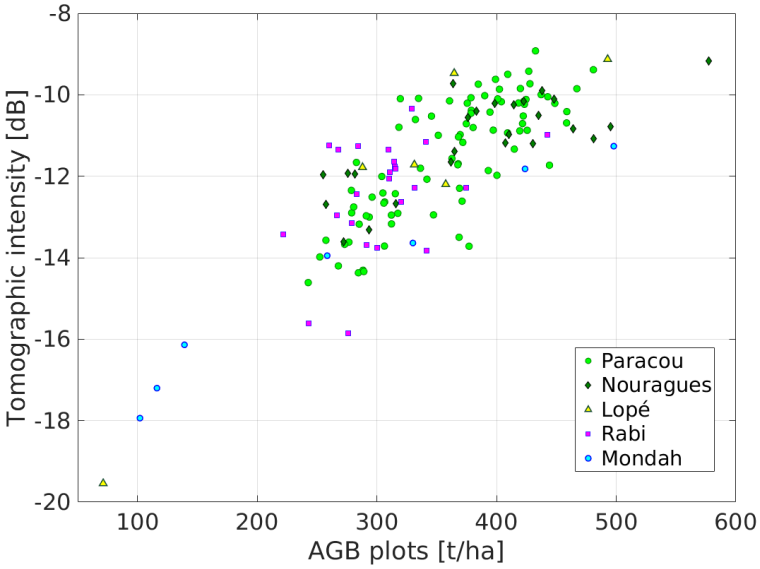

Fig. 4. Plot of HV backscatter intensity at height 30 m above the ground measured by tomography against *in situ* AGB in 1 ha plots at tropical forest sites investigated during the TropiSAR (Paracou and Nouragues) and AfriSAR (Lopé, Rabi, Mondah) campaigns.

The value of tomography for estimating AGB in boreal and temperate forests is less clear, since (a) these forests in general have smaller heights than in the tropics (so it is more problematical to isolate the signal from a canopy layer without corruption by a ground contribution, given the roughly 25 m vertical resolution of the tomographic product from BIOMASS), and (b) the double bounce mechanism appears to be important in recovering the AGB of boreal forests. Hence ground cancellation (which also cancels double bounce scattering, since this appears at ground level in the tomographic image) may noto help biomass estimation in such forests, and the preferred algorithm for BIOMASS in these cases is still not fixed. Recent results indicate that ground cancellation improves results in Krycklan, but not in Remningstorp, most likely because it suppresses direct ground backscattering, which is unrelated to AGB but is of higher relative importance in Krycklan due to the pronounced topography.

5.2 Estimating forest height

Forest height estimates will be available throughout the Tomographic and Interferometric Phases, in the latter case using polarimetric interferometric (Pol-InSAR) techniques (Cloude and Papathanassiou,

1998, 2003; Papathanassiou and Cloude, 2001) applied to three polarimetric acquisitions performed in a 3-day repeat-pass interferometric mode. The use of Pol-InSAR to estimate forest height has been demonstrated at frequencies from X- to P-band for a variety of temperate, boreal and tropical sites, with widely different stand and terrain conditions (Praks et al., 2007; Kugler et al., 2014; Hajnsek et al., 2009; Garestier et al., 2008), and several dedicated studies have addressed its likely performance and limitations when applied to BIOMASS data.

Estimation of forest height from Pol-InSAR requires a model that relates forest height to the Pol-InSAR measurements (i.e. primarily to the interferometric coherence at different polarisations and for different spatial baselines) together with a methodology to invert the established model. Most of the established inversion algorithms use the two-layer Random Volume over Ground (RVoG) model to relate forest height to interferometric coherence (Treuhaft et al., 1996). This relies on two assumptions: 1) all polarizations "see" (up to a scalar scaling factor) the same vertical distribution of scatterers in the vegetation (volume) layer; 2) the ground layer is impenetrable, i.e. for all polarizations, the reflectivity of the ground scattering component is given by a Dirac delta function modulated by a polarimetrically dependent amplitude. The RVoG model has been extensively validated and its strong and weak points are well understood. Use of this model to obtain a forest height map is illustrated in Fig. 5 which is derived by inverting P-band Pol-InSAR data acquired during the AfriSAR campaign in February 2017 over the Pongara National Park, Gabon. This site is covered mainly by mangrove forests, which are among the tallest mangrove forests in the world, towering up to 60 m.

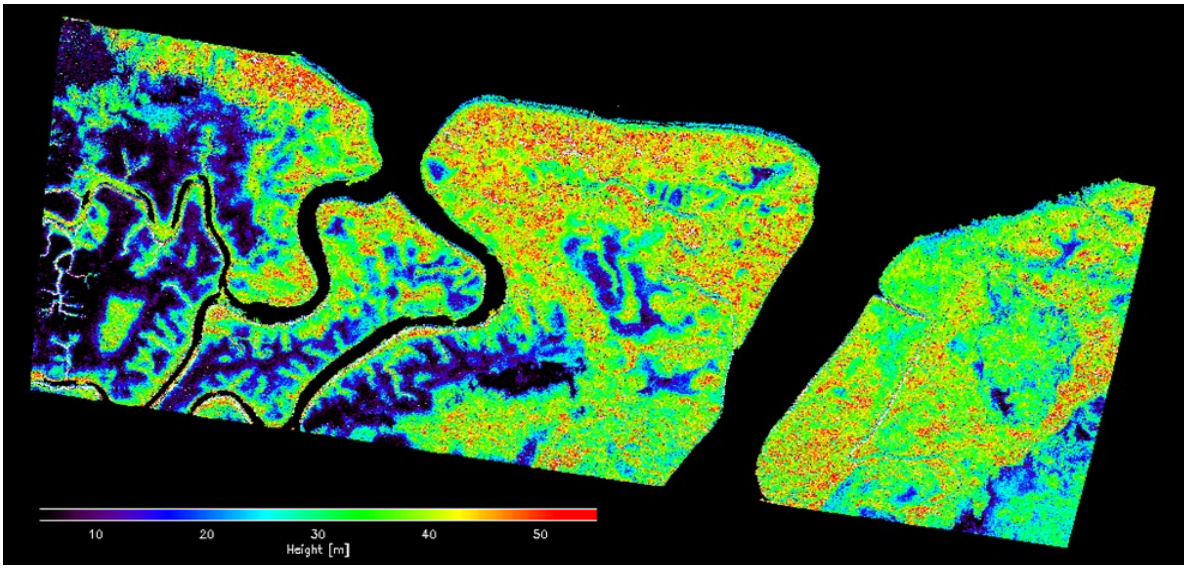

Fig. 5. Forest height map obtained from inverting P-band Pol-InSAR data acquired over the Pongara National Park, Gabon, in the framework of the AfriSAR campaign in February 2017.

The main challenge for BIOMASS is therefore the development of an inversion formulation able to provide unique, unbiased and robust height estimates, and which accounts for: 1) the scattering characteristics at P-band, since the limited attenuation by the forest canopy means that a ground scattering component is present in all polarisations; 2) the constraints imposed by the BIOMASS configuration, both the 6 MHz bandwidth and the fact that some temporal decorrelation is inevitable in the repeat-pass mode (Lee et al., 2013; Kugler et al., 2015). To meet this challenge a flexible multi-baseline inversion scheme has been developed that allows the inversion of the RVoG model by including: 1) a polarimetric three-dimensional ground scattering component; 2) a vertical distribution of volume scattering that can adapt to high (tropical) and low (boreal) attenuation scenarios; 3) a scalar temporal decorrelation that accounts for wind-induced temporal decorrelation of the vegetation layer. The inversion can then be performed using the three polarimetric acquisitions in the Interferometric Phase, allowing global forest height maps to be produced every 7 months.

The main limitations in generating the forest height product arise not from the inversion methodology but from the 6 MHz bandwidth, which constrains the generation of large baselines as well as the spatial resolution of the data, and the low frequency, which reduces the sensitivity to forest height in certain sparse forest conditions. On the other hand, the low frequency will provide high temporal stability over the 3-day repeat period of the Interferometric Phase, which is necessary to establish uniqueness and optimum conditioning of the inversion problem.

An alternative approach to estimating forest height is by tracing the upper envelope of the observed tomographic intensities, as reported in Tebaldini and Rocca (2012) and Ho Tong Minh et al. (2016) for boreal and tropical forests, respectively. This has the advantage of being less computationally expensive than model-based inversion, and it can be applied in the absence of a specific model of the forest vertical structure. Importantly, it has been demonstrated using synthetic 6 MHz data simulating BIOMASS

582 acquisitions over boreal forests (Tebaldini and Rocca, 2012). However, this approach will only be
583 possible during the Tomographic Phase of the mission.
584
585 **6. Severe forest disturbance**
586 The BIOMASS disturbance product aims to detect high-intensity forest disturbance (effectively forest
587 clearance) occurring between satellite revisit times. This is a natural extra use of the data gathered for
588 biomass and height estimation, rather than a driver for the BIOMASS mission, and will contribute to
589 the overall capability to measure forest loss from space using optical (e.g., Hansen et al., 2013) and
590 radar sensors (e.g., the pair of Sentinel-1 C-band radar satellites). Changes in the polarimetric
591 covariance matrix caused by deforestation are relatively large; for example, Fig. 1 indicates that γ^0_{hv}
592 changes by 5 dB as biomass decreases from 500 t ha^{-1} to nearly zero, while a change in AGB from 100
593 to 200 t ha^{-1} causes γ^0_{hv} to change by only ~1 dB. Hence change detection is less affected by the
594 statistical variability inherent in the radar signal, allowing the disturbance product to be produced at a
595 spatial resolution of ~50 m, instead of 200 m, as for the biomass and height products.
596 The method proposed for detecting disturbance is firmly rooted in the statistical properties of the 6-look
597 polarimetric covariance data and uses a likelihood ratio (Conradsen et al., 2016) to test, at a given level
598 of statistical significance, whether change has occurred relative to previous acquisitions in each new
599 polarimetric acquisition over forest. Note that this approach does not specify the detection probability,
600 which would require an explicit form of the multi-variate probability distribution function associated
601 with disturbed forest. This would be very difficult to characterise in any general sense because change
602 may affect the covariance matrix in many different ways. Instead it provides a quantitative way to
603 determine how sure we are that change has occurred; in this respect it is closely related to the Constant
604 False Alarm Rate approach to target detection (e.g. Scharf, 1991).
605 A current unknown in this approach is to what extent changes in the covariance matrix of undisturbed
606 forest caused by environmental effects, such as changing soil moisture due to rainfall events, will
607 increase the false detection rate. A further issue is that detections are only sought in forest pixels, so an

accurate initial forest map is required, preferably estimated from the radar data themselves but possibly from some other source; this will be progressively updated after each new acquisition.

Some insight into the performance of this approach can be gained using multi-temporal polarimetric data from PALSAR-2. Fig. 6 shows at the top Pauli format slant range representations of a pair of images gathered on 8 August 2014 and 8 August 2015 (so in this case the time series has length 2), below left the detection of change at 99% significance and below right the pixels at which change occurred marked in red on the image from 2014 (with no forest mask applied). It can be seen that the areas where change was detected occur in the non-forest regions, while detections in the forest regions occur as isolated pixels consistent with the 1% false alarm rate implied by the level of significance of the test.

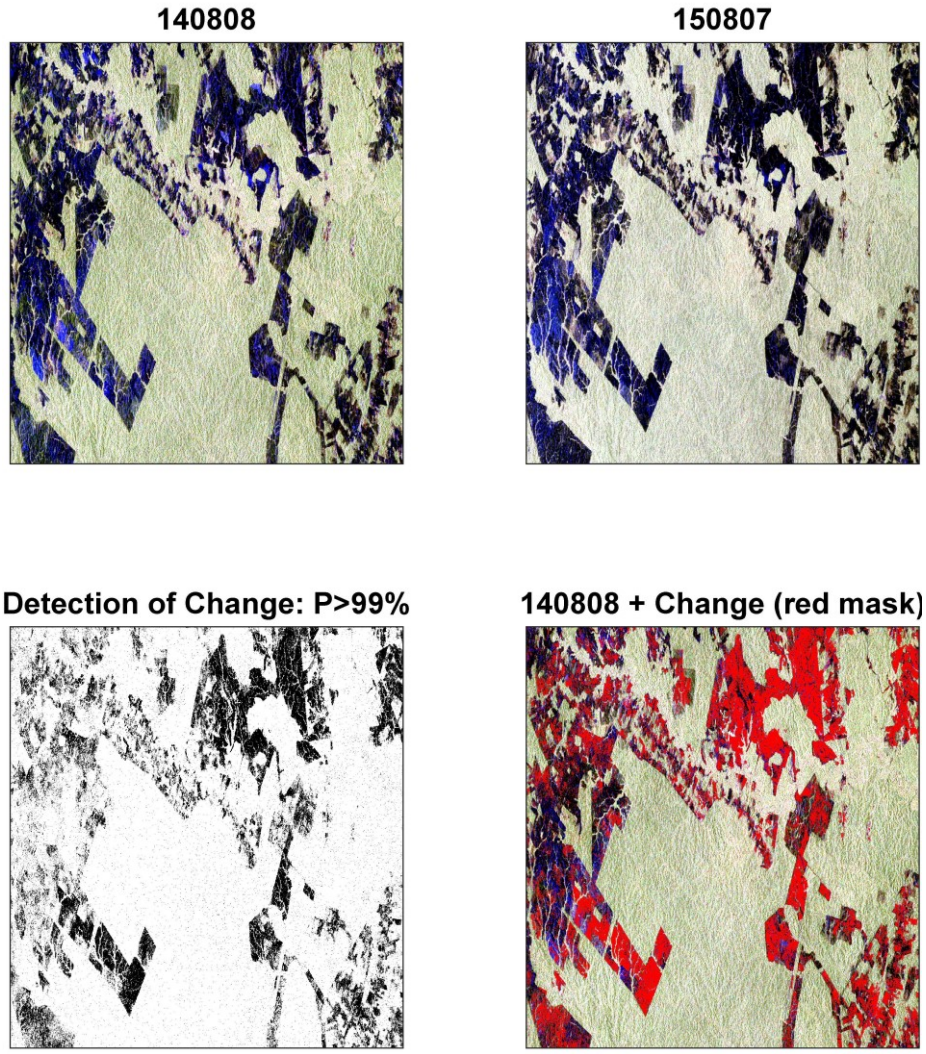

Fig. 6. (Top) Pair of repeat-pass PALSAR-2 images acquired on 8 August 2014 and 7 August 2015 displayed in Pauli image format (red = HH + VV; blue = HH - VV; green = 2HV) and slant range geometry. (Bottom left) Detection of change at 99% significance level; changed pixels are marked as black. (Bottom right) Image from 8 August 2014 with changed pixels marked as red.

7. In situ and lidar reference biomass data

Although the model-based inversion proposed for estimating biomass (Section 5.1) minimises the need for *in situ* reference data, such data are critical for algorithm development and testing, investigation of regression-based approaches, and product calibration and validation. The BIOMASS mission faces three major challenges in providing these supporting data: (i) the key region where reference data are needed is the tropics, but high quality biomass data are available at only a very limited number of tropical sites; (ii) biomass will be estimated at a scale of 4 ha (200 m by 200 m pixels) but most plot data are available at scales of 1 ha or less and the geographical locations of the plots is often not known to high accuracy; (iii) because of SOTR restrictions (Section 2), reference sites in the temperate and boreal zones will need to be outside N America and Europe.

ESA are addressing challenge (i) and (ii) by working with existing networks to develop suitable extensive *in situ* reference data before launch through the Forest Observation System (http://forest-observation-system.net/). A further encouraging development is the ESA-NASA initiative to collaborate in developing the *in situ* data requirements for GEDI, BIOMASS and NISAR. Co-operation along these lines is already in evidence from joint contributions to the AfriSAR campaign by ESA and NASA. As regards (iii), for the temperate zone, southern hemisphere sites, e.g. in Tasmania, would be suitable, while Siberia is the most desirable region for the boreal zone. However, concrete plans to gather *in situ* data in these regions are not currently in place.

An important complement to *in situ* data that helps to address challenge (ii) is airborne lidar data. This can provide a forest height map and information on canopy structure which, when combined with field data, allows biomass to be estimated. Lidar data offer many advantages, including:

- A scanning lidar provides a relatively fine scale and accurate map of biomass, which can be aggregated to the 4 ha resolution cell of BIOMASS (this will allow the effects of variability in

biomass at sub-resolution size to be assessed). Precision at this scale is typically below 10% and the vast majority of relevant studies indicate that the associated pan-tropical allometry (Chave et al. 2014) has negligible bias.

- Lidar mapping can cover landscapes with a wide range of biomass levels and different forest conditions (degraded, regrowth, selectively logged, etc.).
- Forest height with fine resolution (around 1 m) can be estimated at the same time as biomass.

Hence the validation strategy for BIOMASS will involve a combination of *in situ* reference forest plots and lidar-derived biomass/height maps.

8. Exploiting BIOMASS data in carbon cycle and climate analysis

Although the primary objectives of BIOMASS are to reduce the major uncertainties in carbon fluxes linked to Land Use Change, forest degradation and regrowth and to provide support for international agreements (UNFCCC & REDD+), its products will also play a key role in advancing fundamental knowledge of forest ecology and biogeochemistry. For example, BIOMASS data will help in constraining critical carbon cycle parameters, initialising and testing the land component of carbon cycle and Earth System models (ESMs), and quantifying the forest disturbance regime.

Differences between ESM forecasts of the carbon cycle are currently significant, and lead to major uncertainties in predictions (Exbrayat et al., 2018). These differences have been linked to variations in the internal processing of carbon, particularly in the large pools in biomass and soil organic matter (Friend et al. 2014). Linking biomass mapping to estimates of net primary production (NPP) provides a constraint on the turnover rate of the biomass pool, a critical model diagnostic (Carvalhais et al., 2014; Thurner et al., 2014). A recent study (Thurner et al., 2017) found observed boreal and temperate forest carbon turnover rates up to 80% greater than estimates from global vegetation models involved in the Inter-Sectoral Impact Model Intercomparison Project (ISI-MIP) (Warszawski et al., 2014). The relative difference between modelled and observed values is shown in Fig. 7, where the red boxes indicate regions analysed in Thurner et al. (2017) in order to explain these discrepancies. In the boreal zone (boxes b1 - 4) they were mainly attributed to the neglect of the effects of frost damage on mortality in

672 the models, while most of the models did not reproduce observation-based relationships between
673 mortality and drought in temperate forest transects (boxes t1 - 3).
674

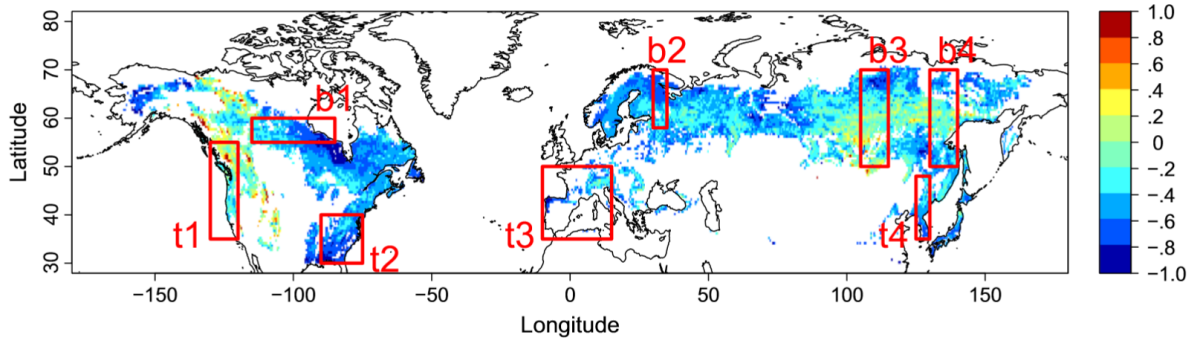

675

676 **Fig 7.** Relative difference between modelled carbon turnover rates and turnover rates inferred from
677 observations. 1.0 means modelled rate is 100% higher (from Thurner et al., 2017). Red boxes labelled
678 b (boreal) and t (temperate) were analysed further in Thurner et al. (2017) to explain these discrepancies
679 (figure reproduced courtesy of Martin Thurner).

680 The more accurate estimates from BIOMASS, particularly over the tropical belt, will greatly improve
681 estimation of turnover across the tropics (Bloom et al., 2016). This information will support improved
682 parameterisation of carbon cycling for ESMs, allowing identification of regional variations in carbon
683 turnover currently missing from tropical plant functional types (Exbrayat et al., 2018a). A sensitivity
684 analysis performed using the CARDAMOM system (Bloom et al., 2016; Exbrayat et al. 2018b)
685 indicates an average reduction of 49.5 ± 29.2% (mean ± 2 std) in the 95% confidence interval of the
686 estimated vegetation carbon turnover time when the recent pan-tropical biomass map due to Avitabile
687 et al. (2016) is assimilated. The analysis shows how this error reduction has clear spatial variability with
688 latitude and between continents (Fig. 8).
689 Another component of uncertainty in ESMs is in their initialisation of biomass stocks, arising from the
690 paucity of data in the tropics, Land Use Change and internal model steady states. Data from BIOMASS
691 will provide the modelling community with a compelling resource with which to understand both steady
692 state and transient forest carbon dynamics. Observations of the disturbance regime will constrain
693 modelling of both natural processes of disturbance and mortality and the role of humans (Williams et

al., 2013). The potential for BIOMASS to monitor degradation (partial loss of biomass) will be critical for modelling the subtle and slow processes of carbon loss associated with forest edges, fires and human communities (Ryan et al, 2012; Brinck et al., 2017).

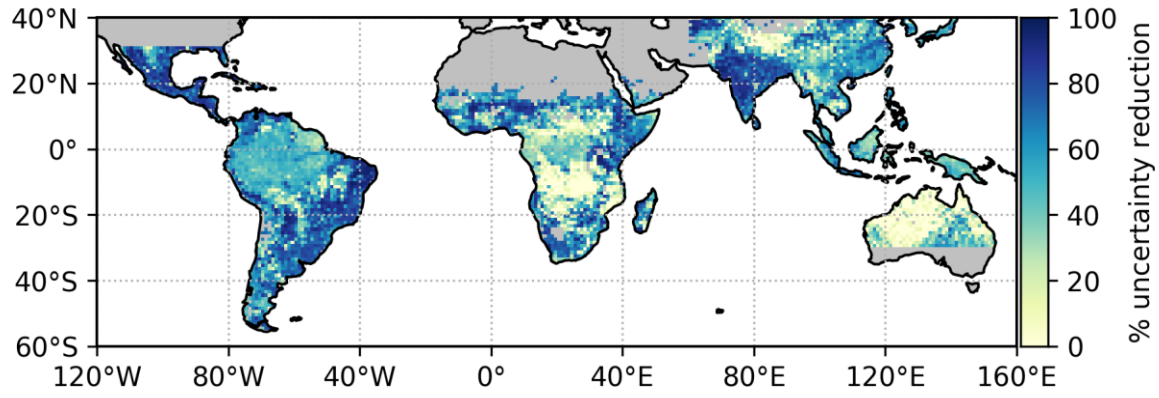

Fig. 8. The relative reduction in the size of the 95% confidence interval of estimated vegetation carbon turnover times when using a prior value for biomass at each pixel compared to a run without a biomass prior. Turnover times were estimated using the CARDAMOM system. The darker areas show where reduction in relative uncertainty is largest.

Repeated measurements of biomass will allow significant improvements in global monitoring of forest dynamics, and analysis of associated carbon cycling at fine spatial scales. Current biomass maps (e.g., Saatchi et al., 2011) provide maps of stocks at a fixed time (or combine observations from several times). While such data help to constrain the steady state biomass, relevant at regional scales (~1º), they give little information on the dynamics of forests at finer (ha to km^2) scales over time. BIOMASS will allow detailed, localised, and temporally resolved analyses of forest dynamics to be constrained. The value of such detailed information has been illustrated in a site level analysis for an aggrading forest in North Carolina (Smallman et al., 2017). Using *in situ* carbon stock information as a baseline, the analysis showed that a model analysis constrained purely by assimilation of 9 sequential annual biomass estimates (corresponding to the BIOMASS scenario, with 1 estimate in the Tomographic Phase and 8 in the Interferometric Phase) together with time series of Leaf Area Index (LAI, e.g. from an operational satellite like Sentinel-2) led to significantly smaller bias and narrower confidence intervals in biomass increment estimates than when LAI and just one biomass estimate, or only management information,

were assimilated. Bias in estimated carbon use efficiency (the ratio of NPP to gross primary production) was also significantly reduced by repeated biomass observations. This indicates the potential of BIOMASS to improve significantly our knowledge of the internal processing of carbon in forests.

9. Secondary objectives

BIOMASS will be the first P-band SAR in space and thus will offer previously unavailable opportunities for measuring properties of the Earth. As a result, mission planning includes provision for several secondary objectives, including mapping sub-surface geology, measuring terrain topography under dense vegetation, estimating glacier and ice sheet velocities and investigating properties of the ionosphere.

9.1 Sub-surface geology

In very dry environments, long wavelength SAR is able to probe the sub-surface down to several metres, as was demonstrated at L-band (1.25 GHz) during the first Shuttle Imaging Radar SIR-A mission (Elachi et al., 1984), which revealed buried and previously unknown palaeo-drainage channels in southern Egypt (McCauley et al., 1982; Paillou et al., 2003). More complete L-band coverage of the eastern Sahara acquired by the JAXA JERS-1 satellite was used to produce the first regional-scale radar mosaic covering Egypt, northern Sudan, eastern Libya and northern Chad, from which numerous unknown crater structures were identified (Paillou et al., 2006). In 2006, JAXA launched the Advanced Land Observing Satellite (ALOS-1), carrying a fully polarimetric L-band SAR, PALSAR, which offered higher resolution and much better signal to noise ratio than JERS-1. This provided an unprecedented opportunity to study the palaeo-environment and palaeo-climate of terrestrial deserts (Paillou et al., 2010), and led to the discovery of two major palaeo-rivers in North Africa: the Kufrah river, a 900 km long palaeo-drainage system, which in the past connected southeastern Libya to the Gulf of Sirt (Paillou et al., 2009; Paillou et al., 2012), and the Tamanrasett River in Mauritania, which connected a vast ancient river system in the western Sahara to a large submarine channel system, the Cap Timiris Canyon (Skonieczny et al., 2015). Besides its value in studying the past climates of desert regions, the sub-surface imaging capability of L-band SAR also helps to build more complete and accurate geological maps in support of future water prospecting in arid and semi-arid regions (Paillou, 2017).

Deeper probing of the sub-surface requires longer radar wavelengths: while L-band can penetrate 1-2 m into dry sand, a P-band system should be able to probe down to more than 5 m. In June 2010, the first ever airborne P-band SAR campaign over the Sahara was conducted at a desert site in southern Tunisia using the SETHI system developed by ONERA (Paillou et al., 2011). Figure 9 shows a comparison between an ALOS-2 L-band scene and a P-band scene acquired by SETHI over the Ksar Ghilane oasis, an arid area at the border between past alluvial plains and present day sand dunes.. The P-band data better reveal the sub-surface features under the superficial sand layer because of the higher penetration depth and lower sensitivity to the covering sand surface. A two-layer scattering model for the surface and sub-surface geometry is able to reproduce both the L- and P-band measured backscatter levels, and indicates that the backscatter from the sub-surface layer is about 30 times weaker than from the surface at L-band, while at P-band the sub-surface contribution is about 30 times stronger than that from the surface. As a result, the total backscatter is comparable at P- and L-band, as the data show, but the P-band return is dominated by the sub-surface layer (Paillou et al., 2017). Hence BIOMASS should be a very effective tool for mapping sub-surface geological and hydrological features in arid areas, offering a unique opportunity to reveal the hidden and still unknown history of deserts.

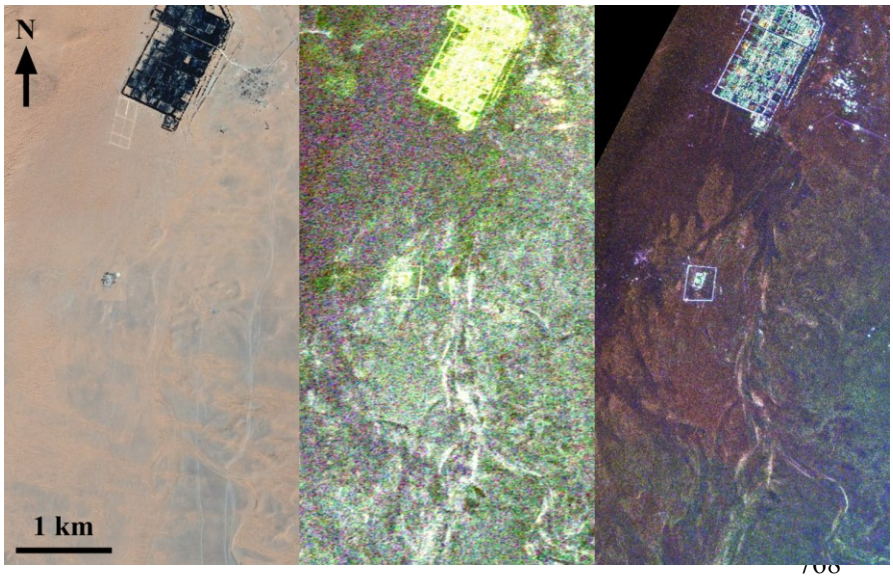

Figure 9. Left: SPOT image of the Ksar Ghilane oasis region in southern Tunisia: palaeo-channels are hidden by aeolian sand deposits. Middle: ALOS-2 L-band radar image, showing sub-surface features but blurred by the return from the superficial sand layer. Right: SETHI P-band radar image, clearly revealing sub-surface hydrological features.

9.2 Terrain topography under dense vegetation

As an integral part of its ability to make height-resolved measurements of the backscatter in forest canopies, the tomographic phase of the mission will gain access to the ground phase, and hence will be able to derive a true Digital Terrain Model (DTM) that is unaffected by forest cover (Mariotti d'Alessandro and Tebaldini, 2018) and expected to have a spatial resolution of ca. 100 m x 100 m. This contrasts with the Digital Elevation Models (DEMs) produced by radar sensors at higher frequencies, such as SRTM (Rodriguez et al., 2015) or Tandem-X (Wessel et al., 2018), in which attenuation and scattering by dense forest canopies cause biases. Since global tomographic acquisitions occupy the first phase of the mission, this improved DTM will be available early in the Interferometric Phase, and will be used to improve the products based on Pol-InSAR and PolSAR.

9.3 Glacier and ice sheet velocities

The velocity fields of glaciers and icesheets can be measured using two classes of SAR techniques: differential SAR Interferometry (DInSAR) (Massonnet et al., 1993) and offset tracking (Gray et al., 1998; Michel & Rignot, 1999). These techniques measure the ice displacement between two observations and require features in the ice or coherence between the observations. BIOMASS has the potential to supplement ice velocity measurements from other SAR missions, since its left-looking geometry with an inclination angle larger than 90° means that the polar gap in Antarctica will be smaller than for most other SAR missions, which are right-looking. The polar gap will be larger in Greenland, but the Greenland ice sheet cannot be mapped due to SOTR restrictions. The primary advantage of BIOMASS is the higher coherence and longer coherence time resulting from the lower frequency of BIOMASS compared to all other space-based SAR systems. Its longer wavelength with deeper penetration into the firn ensures less sensitivity to snowfall, surface melt and aeolian processes (Rignot,

2008). This is seen when comparing L-band and C-band results (Rignot, 2008; Boncori et al., 2010), and explains the long coherence time observed in airborne P-band data acquired by the Danish Technical University POLARIS SAR in the percolation zone of the Greenland ice sheet (Dall et al. 2013).

The range and azimuth components of the ice velocity field will most likely be measured with differential SAR interferometry (DInSAR) and offset tracking, respectively. At lower latitudes two velocity components might instead be obtained by combining DInSAR from ascending and descending orbits, since the range resolution of BIOMASS is too coarse for offset tracking to provide the range component (Dall et al. 2013). Generally DInSAR ensures less noisy results, and phase unwrapping is facilitated by the fact that the fringe rate of BIOMASS DInSAR data will be 1/12 of that of Sentinel-1 data, assuming a 6-day baseline in both cases. The very low ice velocities in the interior of Antarctica call for a long temporal baseline, but a 70-day baseline has been successfully used at C-band (Kwok et al., 2000), and therefore sufficiently high P-band coherence is not unlikely with the 228-day baseline provided by the BIOMASS observation cycle. However, ionospheric scintillation is severe at high latitudes, and without accurate correction will corrupt the ice velocity maps, possibly prohibitively. Assessment of whether proposed correction techniques (Kim et al., 2015; Li et al., 2015) are sufficiently accurate will only be possible when BIOMASS is in orbit.

9.4 Ionospheric properties

A major concern in initial studies for BIOMASS was the effect of the ionosphere on the radar signal, and a crucial factor in the selection of the mission was demonstration that these effects could be compensated or were negligible in the context of the mission primary objectives (Rogers et al., 2013; Rogers and Quegan, 2014). However, correction of ionospheric effects (particularly Faraday rotation, but also scintillation, as noted in Section 9.3) necessarily involves measuring them, which then provides information on the ionosphere. The dawn-dusk BIOMASS orbit will cover major features of the ionosphere, including the fairly quiescent ionosphere at low and mid-latitudes, steep gradients around the dusk-side mid-latitude trough, and large irregularities in the auroral ovals and polar cap. Measurements of ionospheric Total Electron Content, derived from Faraday rotation (Wright et al.,

824 2003) and/or interferometric measurements (Tebaldini et al., 2018), should be possible along the orbit
825 at spatial resolutions of around a km, giving an unprecedented capability to measure these spatial
826 structures and their changes, since they will be viewed every two hours as the orbit repeats.
827
828 **10. The role of BIOMASS in an overall observing system**
829 BIOMASS will have unique capabilities to map biomass in dense forests, but will form only part of the
830 overall system of sensors providing information on forest biomass and biomass change, and more
831 generally on the global carbon cycle. In fact, the next few years will see an unprecedented combination
832 of sensors either dedicated to or capable of measuring forest structure and biomass. Particularly
833 important for their links to BIOMASS will be the Global Ecosystem Dynamics Investigation (GEDI)
834 and NISAR missions.
835 GEDI will be a near infrared (1064 nm wavelength) light detection and ranging (lidar) sensor onboard
836 the International Space Station with a 2-year lifetime from deployment in late 2018. It is focusing on
837 tropical and temperate forests to address three key issues: 1) quantifying the above-ground carbon
838 balance of the land surface; 2) clarifying the role played by the land surface in mitigating atmospheric
839 CO_2 in the coming decades; 3) investigating how ecosystem structure affects habitat quality and
840 biodiversity. GEDI will provide the first sampling of forest vertical structure across all forests between
841 51.5° S and 51.5° N, from which estimates of canopy height, ground elevation and vertical canopy
842 profile measurements will be derived. Further processing of the ~0.0625 ha footprint measurements
843 will then yield estimates of the mean and variance of AGB on a 1 km grid.
844 NISAR (launch 2021) is a joint project between NASA and ISRO (the Indian Space Research
845 Organization) to develop and launch the first dual-frequency SAR satellite, with NASA providing the
846 L-band (24 cm wavelength) and ISRO the S-band (12 cm wavelength) sensors. It will measure AGB
847 and its disturbance and regrowth globally in 1 ha grid-cells for areas where AGB does not exceed 100
848 t/ha, and aims to achieve an accuracy of 20 t/ha or better over at least 80% of these areas. Its focus is
849 therefore on lower biomass forests, which constitute a significant portion of boreal and temperate forests
850 and savanna woodlands. NISAR will give unprecedented L-band coverage in space and time, being

able to provide HH and HV observations every 12 days in ascending and descending orbits and covering forests globally every 6 days. The mission is also designed to give global interferometric SAR measurements for surface deformation and cryosphere monitoring.

These three missions have significant overlaps in science objectives and products, but focus on different observations, cover different regions, and retrieve different components of AGB at different spatial and temporal scales. Their complementary nature is brought out by Fig. 10, which shows the coverage of the three sensors on a map indicating approximate mean AGB. BIOMASS will focus on tropical and sub-tropical woodlands at 4 ha resolution (though will also cover the temperate and boreal forests of Asia and the southern hemisphere), NISAR will give global coverage at 1 ha resolution but with AGB estimates limited to areas where AGB < 100 t/ha, and GEDI will cover the full range of AGB, but with sample footprints limited to lie within ±51.5° latitude. Hence without the data from all three missions, wall-to-wall estimation of global forest biomass will not be possible. There will, however, still be lack of temporal and/or spatial coverage in regions where BIOMASS cannot operate because of SOTR exclusions and where AGB exceeds the 100 t/ha threshold for NISAR.

For lower values of AGB (less than about 50 t/ha) P-band measurements will be much more affected by soil conditions than L-band, and NISAR should provide more accurate AGB estimates. The high temporal frequency of NISAR observations will also allow the effects of soil moisture changes and vegetation phenology to be mitigated. Currently the theoretical basis of the algorithms proposed for NISAR and BIOMASS are the same (Truong-Loi et al., 2015), which offers the possibility of a combined L- and P-band algorithm that optimises the capabilities of each. In addition, GEDI forest height and biomass products will be available before the NISAR and BIOMASS missions, so can help to initialize their algorithms and validate their products. GEDI estimates of the vertical structure of forests will also be of enormous value in interpreting the BIOMASS Pol-InSAR and tomographic measurements and in producing a consistent forest height and digital terrain model at fine spatial scale (around 1 ha). Conversely, height or backscatter products from NISAR and BIOMASS missions can provide information on the spatial variability of forest structure and biomass; this may be used in future

reprocessing to improve both the algorithms that form the GEDI gridded height and biomass products and the resolution of these products.

Hence the three sensors will be highly complementary, and their combination will provide an unparalleled opportunity to estimate forest AGB, height and structure globally with unprecedented accuracy, spatial resolution and temporal and spatial coverage.

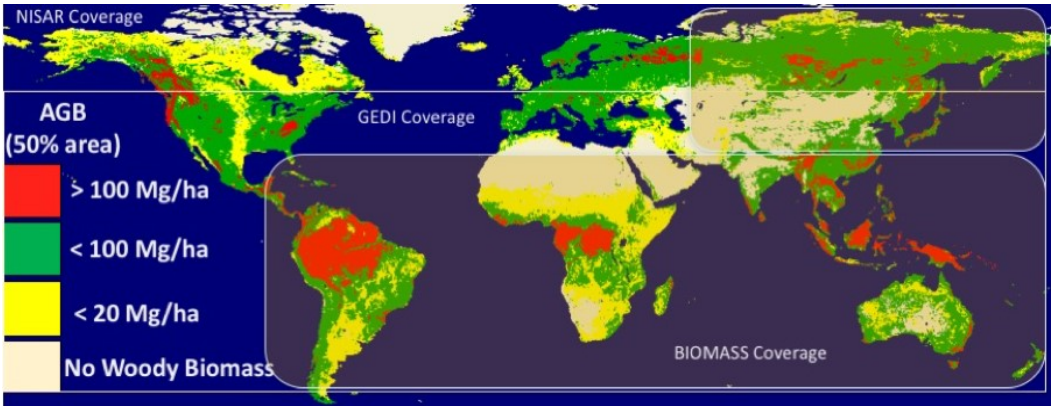

Fig. 10. Coverage of ESA and NASA-ISRO satellite measurements of forest structure and above-ground biomass (AGB). The background shows the global coverage area of NISAR, which will be sensitive to AGB values < 100 t/ha (green and yellow). BIOMASS coverage includes the tropical belt, the temperate and boreal zones of Asia, and the southern hemisphere, while the GEDI Lidar will sample latitudes between ± 51.5°. These two sensors will cover the full range of forest AGB providing measurements where AGB >100 t/ha (red), so inaccessible to NISAR.

Discussion

Along with its role in quantifying the biomass and its change, it is important to realize that the BIOMASS instrument, particularly in its interferometric and tomographic modes, is capable of producing global measures of important forest properties that are simply unavailable for almost all of the Earth. Some of these are practical measurements whose value has been known for years. For example, in forestry the ability to predict yield or increase in biomass is increased greatly when one knows both mass and height, so much so that tree height has been used in yield-table-based forestry to quantify the so-called site-index, the quality of a site for forest enterprise. Hence the information from the BIOMASS satellite and

the modern digital offspring of classic forestry yield tables could be used to make informed estimates of expected net production of forest biomass. In similar vein, Section 8 notes how the combination of biomass with NPP allows the turnover time of carbon within forest vegetation to be estimated. Both examples illustrate that although forest biomass, height, structure and change are all individually important, their full significance for climate, carbon cycle, biodiversity, resource management, etc., is only fully realised when they are combined with each other and with other sources of information.

This perception of biomass as a key variable within a wider information system is implicit in the recognition of AGB as an ECV (GCOS, 2017). More explicit analysis of its function within a carbon information and management system is provided by the Group on Earth Observations (GEO) (Ciais et al., 2010) and the response to this report in the CEOS Strategy for Carbon Observations from Space (CEOS, 2014). In particular, the CEOS report (Fig. 2.3 and Table 2.1 of the report) indicates where biomass fits within the set of key GEO satellite requirement areas and core GEO observational elements necessary to quantify the current state and dynamics of the terrestrial carbon cycle and its components. Central to the GEO Carbon Strategy is the combination of data and carbon cycle models, not least because models provide the only way in which the many available space-based and *in situ* measurements can be integrated into a single consistent structure for performing carbon flux calculations.

There are many possible forms for these models but data can interact with them in essentially four ways: by providing estimates of current model state variables, estimates of model parameters, tracking of processes and testing of model predictions. In addition, data and models can be even more tightly bound by combining them in a data assimilation structure where both are regarded as sources of information whose relative contribution to carbon flux estimates is weighted by their uncertainty. There are already significant developments in exploiting biomass data in these ways, for example initializing the age structure of forests when estimating the European carbon balance (Bellassen et al., 2011), estimating carbon turnover time (Thurner et al., 2017), testing Dynamic Global Vegetation Models (Cantú et al., 2018), and full-scale data assimilation (Bloom et al., 2016). Further progress in this direction is to be expected as we move towards launch in 2022.

Conclusions

BIOMASS mission will be the first space-based P-band radar, and this completely new view from space will yield both predictable and unforeseen opportunities to learn about the Earth and its dynamics. Within the operational constraints imposed by the Space Object Tracking Radar system (Section 2) the 5-year mission will provide global mapping of forest AGB, height and change at 200 m spatial resolution by combining three different radar techniques, each of them innovative. This is the first space-based radar mission for which all observations will be fully polarimetric, which is necessary both to recover biomass information and to correct ionospheric effects. Even more innovative will be this first systematic use of Pol-InSAR to measure forest height globally, and the first use of SAR tomography to identify the vertical structure of forests globally. In parallel with these major technological developments, considerable progress is being made in developing new understanding and quantitative methods that will allow these measurements to be exploited in carbon cycle and climate models. This link between measurements and models forms an essential part of meeting the primary objective of the BIOMASS mission, which is to determine the worldwide distribution of forest AGB in order to reduce the major uncertainties in calculations of carbon stocks and fluxes associated with the terrestrial biosphere, including carbon fluxes associated with Land Use Change, forest degradation and forest regrowth. Of major mutual advantage in meeting this objective will be the information provided by other space missions flying within the next five years, for which pride of place goes to GEDI and NISAR, but supplemented by optical and other radar missions. Of great importance is that the structures for making use of these new data in carbon cycle and climate models are being developed and implemented.

The physical and technical capabilities embedded in the BIOMASS mission in order to measure biomass can be turned to many other uses. At present, known applications include sub-surface imaging in arid regions, estimating glacier and icesheet velocities, and production of a true DTM without biases caused by forest cover. An originally unforeseen application arising from the need to correct the radar signal for ionospheric effects is to exploit the high sensitivity of the P-band signal to Total Electron Content to estimate ionospheric properties and changes along the satellite's dawn-dusk orbit. This is likely to be just one amongst many novel uses of the BIOMASS data, whose scope will only become clear once BIOMASS is in orbit.

Acknowledgements

This work was in part supported by the UK National Environment Research Council National Centre for Earth Observation (NCEO).

References

Antonarakis, A.S., Saatchi, S.S., Chazdon, R.L. & Moorcroft, P.R. (2011). Using Lidar and radar measurements to constrain predictions of forest ecosystem structure and function. *Ecological Applications, 21*(*4*), 1120–1137.

Askne, J. I. H., Soja, M. J., and Ulander, L. M. H. (2017). Biomass estimation in a boreal forest from TanDEM-X data, lidar DTM, and the interferometric water cloud model, *Remote Sensing of Env.*, *196*, 265-278, doi:org/10.1016/j.rse.2017.05.010.

Avitabile, V., Herold, M., Heuvelink, G. B. M., Lewis, S. L., Phillips, O. L., Asner, G. P., et al. (2016). An integrated pan-tropical biomass map using multiple reference datasets, *Glob. Change Biol. 22*(*4*), 1406-1420, doi: 10.1111/gcb.13139.

Baccini, A., Goetz, S. J., Walker, W. S., Laporte, N. T., Sun M., Sulla-Menashe, D., et al. (2012). Estimated carbon dioxide emissions from tropical deforestation improved by carbon-density maps. *Nature Clim. Change, 2*, 182-185, doi:110.1038/nclimate1354.

Baccini, A., Walker, W., Carvalho, L., Farina, M., Sulla-Menashe, D., Houghton, R. A. (2017). Tropical forests are a net carbon source based on aboveground measurements of gain and loss, *Science, 358*(*6360*), 230-234, doi:10.1126/science.aam5962.

Bai, Y., Tebaldini, S., Ho Tong Minh, D., and Yang, W. (2018). An empirical study on the impact of changing weather conditions on repeat-pass SAR tomography," *IEEE Jnl. Selected Topics in Applied Earth Observations and Remote Sensing*, 1–7.

983 Bellassen, V., Viovy, N., Luyssaert, S., Le Maire, G., Schelhaas, M.-J. and Ciais, P. (2011).
984 Reconstruction and attribution of the carbon sink of European forests between 1950 and 2000, *Global*
985 *Change Biology*, *17*, 3274–3292, doi: 10.1111/j.1365-2486.2011.02476.x.

986 Bloom AA, Exbrayat J-F, van der Velde I.R., Feng L, Williams, M. (2016). The decadal state of the
987 terrestrial carbon cycle: Global retrievals of terrestrial carbon allocation, pools, and residence times,
988 *PNAS*, *113*(*5*), 1285-1290, doi:pnas.1515160113.

989 Boncori, J.P.M., Dall, J., Ahlstrøm, A.P., Andersen, S.B. (2010). Validation and operational
990 measurements with SUSIE: a SAR ice motion processing chain developed within PROMICE
991 (Programme for Monitoring of Greenland Ice-Sheet), *Proc. ESA Living Planet Symposium, Bergen*.

992 Bouvet, A., Mermoz, S., Le Toan, T., Villard, L., Mathieu, R., Naidoo, L., and Asner, G. P. (2018). An
993 above-ground biomass map of African savannahs and woodlands at 25 m resolution derived from ALOS
994 PALSAR, *Remote Sens. Env.*, *206*, 156–173.

995 Brinck, K., Fischer, R., Groeneveld, J., Lehmann, S., De Paula, M.D., et al. (2017). High resolution
996 analysis of tropical forest fragmentation and its impact on the global carbon cycle. *Nature*
997 *Communications, 8*, 14855

998 Cairns, M.A., Brown, S., Helmer, E.H., & Baumgardner, G.A. (1997). Root biomass allocation in the
999 world's upland forests. *Oecologia, 111*, 1–11.

1000 Cantú, A. G., Friele, K., Reye, C. P.O., Ciais, P., Chang, J., Ito, A., et al. (2018). Evaluating changes
1001 of biomass in global vegetation models: the role of turnover fluctuations and ENSO events, *Environ.*
1002 *Res. Lett., 13*, 075002.

1003 Carreiras, J. M. B., Quegan, S., Le Toan, T., Ho Tong Minh, D., Saatchi, S., Carvalhais, N., et al. (2017).
1004 Coverage of high biomass forests by the ESA BIOMASS mission under defense restrictions, *Remote*
1005 *Sensing of Environment, 196*, 154-162, doi.org/10.1016/j.rse.2017.05.003.

1006 Carvalhais N, Forkel M, Khomik M, Bellarby J, Jung M, Migliavacca M, et al. (2014). Global
1007 covariation of carbon turnover times with climate in terrestrial ecosystems. *Nature, 514*, 213-217.

1008 CEOS (2014). *CEOS Strategy for Carbon Observations from Space; The Committee on Earth*
1009 *Observation Satellites (CEOS) Response to the Group on Earth Observations (GEO) Carbon Strategy.*

1010 Chave, J. (1999). Study of structural, successional and spatial patterns in tropical rain forests using
1011 TROLL, a spatially explicit forest model, *Ecological Modelling*, *124* (*2–3*), 233–254.

1012 Chave, J., Rejou-Mechain, M. , Burquez, A., Chidumayo, E., Colgan, M. S., Delitti, W. B., et al. (2014).
1013 Improved allometric models to estimate the aboveground biomass of tropical trees, *Global Change*
1014 *Biology*, *20*, 3177–3190, doi: 10.1111/gcb.12629.

1015 Ciais, P., Dolman, A. J., Dargaville, R., Barrie, L., Bombelli, A., Butler, J., et al. (2010). *GEO Carbon*
1016 *Strategy*, GEO Secretariat Geneva/FAO, Rome, 48 pp.

1017 Cloude, S. R., and Pottier, E. (1996). A review of target decomposition theorems in radar polarimetry,
1018 *IEEE Trans. Geosci. Remote Sens.*, *34*(*2*), 498–518.

1019 Cloude, S. R., and Papathanassiou, K. P. (1998). Polarimetric SAR interferometry, *IEEE Trans. Geosci.*
1020 *Remote Sensing*, *36*(*5*), 1551-1565.

1021 Cloude S. R. and Papathanassiou, K. P. (2003), Three-stage inversion process for polarimetric SAR
1022 interferometry, *IEE Proc. Radar, Sonar and Navigation*, *150*(*3*), 125-134.

1023 Conradsen, K., Nielsen, A. A., Schou, J., and Skriver, H. (2003). A test statistic in the complex Wishart
1024 distribution and its application to change detection in polarimetric SAR data, *IEEE Trans. Geosci.*
1025 *Remote Sensing*, *41*(*1*), 4-19.

1026 Conradsen, K., Nielsen, A. A., and Skriver, H. (2016). Determining the points of change in time series
1027 of polarimetric SAR data, *IEEE Trans. Geosci. Remote Sensing*, *54*(*5*), 3007-3024.

1028 Dall, J., Nielsen, U., Kusk, A., van de Wal, R.S.W. 2013. Ice flow mapping with P-band SAR, *Proc.*
1029 *Int Geosci. Remote Sensing Symp. (IGARSS 2013)*, Melbourne.

1030 Dubois-Fernandez, P., Le Toan, T., Daniel, S., Oriot, H., Chave, J., Blanc, L., et al. (2012). The
1031 TropiSAR airborne campaign in French Guiana: Objectives, description and observed temporal
1032 behavior of the backscatter signal, *IEEE Trans. Geosci. Remote Sensing, 50*(*8*), 3228-3241.

1033 Elachi, C., Roth, L. E., and Schaber, G. G. (1984). Spaceborne radar sub-surface imaging in hyperarid
1034 regions, *IEEE Trans. Geosci. Remote Sensing*, vol. GE-22, pp. 383-388,.

1035 European Space Agency (2008). *BIOMASS: Candidate Earth Explorer Core Missions - Reports for*
1036 *Assessment*; ESA SP-1313-2, Mission Science Division, ESA-ESTEC, Noordwijk, the Netherlands,
1037 ISSN 0379-6566, 122 pp.

1038 European Space Agency (2012). *Report for Mission Selection: Biomass*. Science authors: Quegan, S.,
1039 Le Toan T., Chave, J., Dall, J., Perrera, A., Papathanassiou, et al., ESA SP 1324/1 (3 vol. series),
1040 European Space Agency, Noordwijk, the Netherlands, pp. 193.

1041 European Space Agency (2015). *Biomass Mission Requirements Document*, EOP-SM/1645.

1042 Exbrayat, J.-F., Bloom, A. A., Falloon, P., Ito, A., Smallman, T. L., & Williams, M. (2018a). Reliability
1043 ensemble averaging of 21st century projections of terrestrial net primary productivity reduces global
1044 and regional uncertainties. *Earth System Dynamics*, *9*(*1*), 153–165, https://doi.org/10.5194/esd-9-153-
1045 2018.

1046 Exbrayat, J.-F., Luke Smallman, T., Anthony Bloom, A., Hutley, L. B., & Williams, M.
1047 (2018b). Inverse determination of the influence of fire on vegetation carbon turnover in the
1048 pantropics. *Global Biogeochemical Cycles*, *32*, 1776–1789. https://doi.org/10.1029/2018GB005925.

1049 FAO. (2006). *Global Forest Resources Assessment 2005*. FAO Forestry Paper 147, United Nations
1050 Food and Agriculture Organization, Rome, Italy.

1051 FAO (2008). UN Collaborative Programme on Reducing Emissions From Deforestation And Forest
1052 Degradation in Developing Countries (UN-REDD). FAO, UNDP, UNEP.

1053 FAO (2009) Assessment of the status of the development of the standards for the Terrestrial Essential
1054 Climate Variables, GTOS Secretariat, UN Food and Agriculture Organisation, Rome, Italy.

1055 FAO. (2010). *Global Forest Resources Assessment 2010*, United Nations Food and Agriculture
1056 Organization, Rome, Italy. ISBN 978-92-5-106654-6.

1057 FAO (2016). *Global Forest Resources Assessment 2015 Second Edition*, Food and Agriculture
1058 Organization of the United Nations, Rome, ISBN 978-92-5-109283-5.

FAO (2012). *Global Ecological Zones for FAO Forest Reporting: 2010 Update. Forest Resources Assessment Working Paper 179*, Food and Agriculture Organisation of the United Nations, Rome, Italy.

Fransson, J. E. S., Walter, F., and Ulander, L. M. H. (2000). Estimation of forest parameters using CARABAS-II VHF SAR data, *IEEE Trans. Geosci. Remote Sens.*, *38*(*2*), 720–727.

Freeman, A., and Durden, S. (1998). A three-component scattering model for polarimetric SAR data, *IEEE Trans. Geosci. Remote Sens.*, *36*(*3*), 963–973.

Friend, A. D., Lucht, W., Rademacher, T. T., Keribin, R. M., Betts, R., et al. (2014). Carbon residence time dominates uncertainty in terrestrial vegetation responses to future climate and atmospheric CO2. *Proceedings of the National Academy of Sciences of the United States of America, 111*, 3280 – 3285.

Garestier, F., Dubois-Fernandez, P. C., and Papathanassiou, K. P. (2008). Pine forest height inversion using single-pass X-Band Pol-InSAR data, *IEEE Trans. Geosci. Remote Sensing*, *46*(*1*), 59-68.

GCOS (2015). *Status of the Global Observing System for Climate*, GCOS-195, WMO, Geneva, http://www.wmo.int/pages/prog/gcos/Publications/GCOS-195_en.pdf.

GCOS (2017). *The Global ObservingSystem for Climate: implementation needs*, GCOS-200, WMO, Geneva.

Gray, A.L., Mattar, K.E., and Vachon, P.W. (1998). InSAR results from the RADARSAT Antarctic mapping mission data: estimation of data using a simple registration procedure, *Proc. Int Geosci. Remote Sensing Symp. (IGARSS 1998)*, Seattle.

Hajnsek I., Scheiber, R., Ulander, L., Gustavsson, A., Sandberg, G., Tebaldini, S., et al. (2008). *BIOSAR 2007: Technical Assistance for the Development of Airborne SAR and Geophysical Measurements during the BioSAR 2007 Experiment*, Final Report, ESA contract No.: 20755/07/NL/CB.

Hajnsek, I., Scheiber, R., Keller, M., Horn, R., Lee, S., Ulander, L., et al. (2009). *BIOSAR 2008: Final Report*, ESTEC Contract 22052/08/NL/CT-002, 302 pp.

1082 Hajnsek, I., Kugler, F., Lee, S.K., and Papathanassiou, K.P. (2009). Tropical forest parameter
1083 estimation by means of Pol-InSAR: The INDREX-II campaign, *IEEE Trans. Geosci. Remote Sensing*
1084 *47*(*2*), 481-493.

1085 Hansen, M. C., Potapov, P. V., Moore, R., Hancher, M., Turubanova, S. A., Tyukavina, A., et al. (2013).
1086 High-resolution global maps of 21st-century forest cover change, *Science, 15*(*342*), Issue 6160, 850-
1087 853, doi: 10.1126/science.1244693.

1088 Ho Tong Minh, D., Tebaldini, S., Rocca, F., Albinet, C., Borderies, P., Koleck, T., et al. (2012).
1089 Tropiscat: multi-temporal multi-polarimetric tomographic imaging of tropical forest, *Proc. 2012 IEEE*
1090 *International Geosci. Remote Sensing Symp*., Munich, 22-27 July 2012, 7051-7054.

1091 Ho Tong Minh, D., Le Toan, T., Rocca, F., Tebaldini, S., d'Alessandro, M. M., and Villard, L. (2014).
1092 Relating P-band Synthetic Aperture Radar tomography to tropical forest biomass, *IEEE Trans Geosci.*
1093 *Remote Sensing*, *52*(*2)*, 967-979.

1094 Ho Tong Minh, D., Le Toan, T., Rocca, F., Tebaldini, S., Villard, L., Réjou-Méchain, M., Phillips, O.L.,
1095 Feldpausch, T.R., Dubois-Fernandez, P., Scipal, K., Chave, J. (2016). SAR tomography for the retrieval
1096 of forest biomass and height: Cross-validation at two tropical forest sites in French Guiana, *Remote*
1097 *Sensing of Environment*, *175*, 138-147.

1098 IPCC (2007). *IPCC Fourth Assessment Report: Climate Change 2007, The Physical Science Basis*.
1099 Cambridge University Press, Cambridge, UK.

1100 IPCC (2013). *Climate Change 2013: The Physical Science Basis. Contribution of Working Group I to*
1101 *the Fifth Assessment Report of the Intergovernmental Panel on Climate Change* (Stocker, T. F., D. Qin,
1102 G.-K. Plattner, M. Tignor, S. K. Allen, J. Boschung, A. Nauels, Y. Xia, V. Bex and P. M. Midgley
1103 (eds.)). Cambridge University Press, Cambridge, United Kingdom and New York, NY, USA, 1535 pp.

1104 Kim, J.-S., Papathanassiou, K., Scheiber, R., and Quegan, S. (2015). Correction of ionospheric
1105 scintillation induced distortions on polarimetric SAR data, *IEEE Trans. Geosci. Remote Sensing*, doi:
1106 10.1109/TGRS.2015.2431856.

Koleck, T., Borderies, P., Rocca, F., Albinet, C., Ho Tong Minh, D., Tebaldini, S., Hamadi, A.,et al. (2012). TropiSCAT: A polarimetric and tomographic scatterometer experiment in French Guiana forests, *Proc. 2012 IEEE International Geosci. Remote Sensing Symp*., Munich, 22-27 July 2012, 7597-7600, doi: 10.1109/IGARSS.2012.6351869

Kugler, F., Schulze, D., Hajnsek, I., Pretzsch, H., Papathanassiou, K. P. (2014). TanDEM-X Pol-InSAR performance for forest height estimation, *IEEE Trans. Geosci. Remote Sensing*, *52*(*10*), 6404-6422.

Kugler, F., Lee, S-K., Papathanassiou, K. P. (2015). Forest height estimation by means of Pol-InSAR data inversion: the role of the vertical wavenumber, *IEEE Trans. Geosci. Remote Sensing*, *53*(*10*), 5294-5311

Kwok, R., Siegert, M.J., Carsey, F.D. (2000). Ice motion over Lake Vostok, Antarctica: constraints on inferences regarding the accreted ice, *Journal of Glaciology*, 46(155), 689-694.

Labrière, N., Tao, S., Chave, J., Scipal, K., Le Toan, T., Abernethy, K., et al. (2018). In situ reference datasets from the TropiSAR and AfriSAR campaigns in support of upcoming spaceborne biomass missions*, IEEE Jnl. Selected Topics in Applied Earth Observations and Remote Sensing, 11(10)*, 3617-3627, doi: 10.1109/JSTARS.2018.2851606.

Le Quéré, C., Andrew, R. M., Friedlingstein, P., Sitch, S., Pongratz, J., Manning, A. C., et al. (2018). Global Carbon Budget 2017, *Earth Syst. Sci. Data*, *10*, 405-448, doi: 10.5194/essdd-2017-123.

Le Toan T., Quegan, S., Davidson, M., Balzter, H., Paillou, P., Papathanassiou, K., et al. (2011). The BIOMASS mission: Mapping global forest biomass to better understand the terrestrial carbon cycle, *Remote Sens. Env*., *115*, 2850–2860.

Ledo, A., Paul, K. I., Burslem, D. F., Ewel, J. J., Barton, C., Battaglia, M., et al. (2018). Tree size and climatic water deficit control root to shoot ratio in individual trees globally, *New Phytologist*, *217*(*1*), 8-11.

Lee, J.-S., Schuler, D., and Ainsworth, T. (2000). Polarimetric SAR data compensation for terrain azimuth slope variation, *IEEE Trans Geosci. Remote Sensing*, *38*(*5*), 2153–2163.

1132 Lee, S.-K., Kugler, F., Papathanassiou, K. P., and Hajnsek, I. Quantification of temporal decorrelation
1133 effects at L-band for polarimetric SAR interferometry applications (2013). *IEEE Jnl. Selected Topics*
1134 *in Applied Earth Observations and Remote Sensing*, *6*(*3*), 1351-1367.

1135 Lefsky, M. A., Harding, D. J., Keller, M., Cohen, W. B., Carabajal, C., Del Bom Espirito-Santo, F., et
1136 al. (2005). Estimates of forest canopy height and aboveground biomass using ICESat. *Geophysical*
1137 *Research Letters 32*, L22S02, doi:10.1029/2005GL023971.

1138 Lefsky, M. A. (2010). A global forest canopy height map from the Moderate Resolution Imaging
1139 Spectroradiometer and the Geoscience Laser Altimeter System**,** *Geophysical Research Letters 37*(*15*),
1140 doi.org/10.1029/2010GL043622

1141 Li, Z., Quegan, S., Chen, J., and Rogers, N. C. (2015). Performance analysis of Phase Gradient
1142 Autofocus for compensating ionospheric scintillation in BIOMASS P-band SAR data, *IEEE Trans.*
1143 *Geosci. Remote Sensing Letts., 12*(*6*), 1367-1371, doi: 10.1109/LGRS.2015.2402833.

1144 Mariotti d'Alessandro, M., Tebaldini, S., Quegan, S., Soja, M. J., Ulander, L. M. H. (2018).
1145 Interferometric ground notching, *Proc. Int Geosci. Remote Sensing Symp. (IGARSS 2018)*, Valencia.

1146 Mariotti d'Alessandro, M. and Tebaldini, S. (2018). Retrieval of terrain topography in tropical forests
1147 using P-band SAR tomography, *Proc. Int Geosci. Remote Sensing Symp. (IGARSS 2018)*, Valencia.

1148 Mariotti d'Alessandro, M., Tebaldini, S., and Rocca, F. (2013). Phenomenology of ground scattering
1149 in a tropical forest through polarimetric synthetic aperture radar tomography, *IEEE Trans. Geosci.*
1150 *Remote Sensing*, *51*(*8*), 4430-4437.

1151 Meyer, V., Saatchi, S., Clark, D. B., Keller, M., Vincent, G., et al. (2018).Canopy area of large trees
1152 explains aboveground biomass variations across neotropical forest landscapes, *Biogeosciences*, *15*,
1153 3377–3390.

1154 Massonnet, D., Rossi, M., Carmona, C., Adragna, F., Peltzer, G., Feigl, K., Rabaute, T. (1993). The
1155 displacement field of the Landers earthquake mapped by radar interferometry, *Nature*, 364, 138-142.

McCauley, J. F., Schaber, G. G., Breed, C. S., Grolier, M. J., Haynes, C. V., Issawi, B., et al. (1982). Sub-surface valleys and geoarchaeology of the eastern Sahara revealed by Shuttle Radar, *Science*, *218*, pp. 1004-1020,.

Michel, R. & Rignot, E. (1999). Flow of Glacier Moreno, Argentina, from repeat-pass Shuttle Imaging Radar images: comparison of the phase correlation method with radar interferometry. *Journal of Glaciology, 45*(*149*), 93–100.

Mitchard, E. T. A., Saatchi, S. S., Woodhouse, I. H., Nangendo, G., Ribeiro, N. S., and Williams, M. (2009). Using satellite radar backscatter to predict above-ground woody biomass: A consistent relationship across four different African landscapes, *Geophys. Res. Lett*., *36*, Article L23401, doi:10.1029/2009GL040692.

Mitchard, E. T. A., Saatchi, S. S., Baccini, A., Asner, G. P., Goetz, S. J., Harris, N. L., et al., (2013). Uncertainty in the spatial distribution of tropical forest biomass: a comparison of pan-tropical maps. *Carbon Balance and Management*, *8*(*10*), doi:10.1186/1750-0680-8-10.

Mitchard, E. T. A., Feldpausch, T. R., Brienen, R. J. W., Lopez-Gonzalez, G., Monteagudo, A., Baker, T. R., et al., (2014). Markedly divergent estimates of Amazon forest carbon density from ground plots and satellites. *Global Ecol. Biogeogr.*, *23*(*8*), 836-955, doi: 10.1111/geb.12168.

Mokany, K., Raison, R.J., and Prokushkin, A.S. (2006). Critical analysis of root:shoot ratios in terrestrial biomes. *Global Change Biology*, *12*(*1*), 84-96.

Monteith, A. R., and Ulander, L. M. H. (2018). Temporal survey of P- and L-band polarimetric backscatter in boreal forests, *IEEE Jnl. Selected Topics in Applied Earth Observations and Remote Sensing*, *11*(*10*), 3564 – 3577.

Paillou, P., Grandjean, G., Baghdadi, N., Heggy, E., August-Bernex, T., and Achache, J. (2003). Sub-surface imaging in central-southern Egypt using low frequency radar: Bir Safsaf revisited, *IEEE Trans. Geosci. Remote Sensing*, *41*(*7*), 1672-1684.

1180 Paillou, P., Reynard, B., Malézieux, J.-M, Dejax, J., Heggy, E., Rochette, P., et al. (2006). An extended
1181 field of crater-shaped structures in the Gilf Kebir region – Egypt: Observations and hypotheses about
1182 their origin, *Jnl. African Earth Sciences*, *46*, 281-299.

1183 Paillou, P., Schuster, M., Tooth, S., Farr, T., Rosenqvist, A., Lopez, S., et al. (2009). Mapping of a
1184 major paleodrainage system in Eastern Libya using orbital imaging Radar: The Kufrah River, *Earth*
1185 *and Planetary Science Letters*, *277*, 327-333, doi: 10.1016/j.epsl.2008.10.029.

1186 Paillou, P., Lopez, S., Farr, T. and Rosenqvist, A. (2010). Mapping sub-surface geology in Sahara using
1187 L-band SAR: first results from the ALOS/PALSAR imaging radar, *IEEE Journal of Selected Topics in*
1188 *Earth Observations and Remote Sensing*, *3*(*4*), 632-636.

1189 Paillou, P., Ruault du Plessis, O., Coulombeix, C., Dubois-Fernandez, P., Bacha, S., Sayah, N., et al.
1190 (2011). The TUNISAR experiment: flying an airborne P-band SAR over southern Tunisia to map sub-
1191 surface geology and soil salinity," *PIERS 2011*, Marrakesh, Morocco.

1192 Paillou, P., Tooth, S., and Lopez, S. (2012). The Kufrah paleodrainage system in Libya: a past
1193 connection to the Mediterranean Sea?, *C.R. Geoscience*, *344*, 406-414.

1194 Paillou, P. (2017). Mapping palaeohydrography in deserts: contribution from space-borne imaging
1195 radar, *Water*, *9*(*194*).

1196 Paillou, P. Dubois-Fernandez, P., Lopez, S., and Touzi, R. (2017). SAR polarimetric scattering
1197 processes over desert areas: Ksar Ghilane, Tunisia, *POLINSAR*, Frascati, Italy.

1198 Pan, Y., Birdsey, R.A., Fang, J., Houghton, R., Kauppi, P.E., Kurz, W. A., et al. (2011). A large and
1199 persistent carbon sink in the world's forests. *Science*, *333*, 988-993.

1200 Papathanassiou, K. P., Cloude, S. R. (2001). Single-baseline polarimetric SAR interferometry. *IEEE*
1201 *Trans. Geosci. Remote Sensing*, *39*(*11*), 2352-2363.

1202 Persson, H. J., Olsson, H., Soja, M, J., Ulander, L. M. H., and Fransson, J. E. S. (2017). Experiences
1203 from large-scale forest mapping of Sweden using TanDEM-X data, *Remote Sensing*, *9* (*12*),
1204 doi:10.3390/rs9121253.

1205 Philip, M.S. (1994). *Measuring Trees and Forests*, Second Edition, CAB International, Oxon, UK.

1206 Praks, J., Kugler, F., Papathanassiou, K. P., Hajnsek, I., Hallikainen, M. (2007). Tree height estimation
1207 for boreal forest by means of L- and X-band Pol-InSAR and HUTSCAT scatterometer, *IEEE Trans.*
1208 *Geosci. Remote Sensing Letts*., *37*(*3*), 466–470.

1209 Quegan, S., Lomas, M., Papathanassiou, K. P., Kim, J-S., Tebaldini, S., Giudici, D., et al. (2018).
1210 Calibration challenges for the BIOMASS P-band SAR instrument, *Proc. IEEE Int. Geosci. Remote*
1211 *Sensing Symp. (IGARSS 2018)*, Valencia.

1212 Rackham, O., & Moody, J. (1996). *The making of the Cretan landscape*. Manchester University Press.

1213 Rodriguez, E., Morris, C. S., Belz, J. E., Chapin, E. C., Martin, J. M., Daffer, W., et al. (2005). *An*
1214 *assessment of the SRTM topographic products*, Technical Report JPL D-31639, Jet Propulsion
1215 Laboratory, Pasadena, California.

1216 Radkau, J. (2012). *Wood: a history* (Vol. 17). Polity.

1217 Rignot, E. (2008). Changes in West Antarctic ice stream dynamics observed with ALOS PALSAR data,
1218 *Geophysical Research Letters* **35**, L12505, doi:10.1029/2008GL033365, 1–5.

1219 Rogers, N. C., Quegan, S., Kim, J. S. and Papathanassiou, K. P. (2013). Impacts of ionospheric
1220 scintillation on the BIOMASS P-band satellite SAR, *IEEE Trans. Geosci. Remote Sensing, 52*(*1*), doi:
1221 10.1109/TGRS.2013.2255880.

1222 Rogers, N. C., and Quegan, S. (2014). The accuracy of Faraday rotation estimation in satellite Synthetic
1223 Aperture Radar images, *IEEE Trans. Geosci. Remote Sensing, 52*(*8*), 4799 – 4807, doi:
1224 10.1109/TGRS.2013.2284635

1225 Rosenqvist, A., Shimada, M., Suzuki, S., Ohgushi, F., Tadono, T., Watanabe, M., et al. (2014).
1226 Operational performance of the ALOS global systematic acquisition strategy and observation plans for
1227 ALOS-2 PALSAR-2, *Remote Sens. Env. 155*, 3-12, doi.org/10.1016/j.rse.2014.04.011.

1228 Ru, X., Liu, Z., Huang, Z., and Jiang, W. (2016). Normalized residual-based constant false-alarm rate
1229 outlier detection. *Pattern Recognition Letters*, *69*, 1-7.

1230 Ryan C. M., Hill T. C., Woollen E., Ghee C., Mitchard E. T. A. , Cassells G, Grace J, Woodhouse IH,
1231 Williams M. (2012). Quantifying small-scale deforestation and forest degradation in African woodlands
1232 using radar imagery. *Global Change Biology 18*, 243-257.

1233 Saatchi, S.,Marlier, M., Chazdon, R. L., Clark, D B., and Russell, A. (2011). Impact of spatial variability
1234 of tropical forest structure on radar estimation of aboveground biomass, *Remote Sensing of*
1235 *Environment*, *115*(*11*), 2836-2849, doi.org/10.1016/j.rse.2010.07.015.

1236 Saatchi, S. S., Harris, N. L., Brown, S., Lefsky, M., Mitchard, E. T. A., Salas, W., et al., (2011).
1237 Benchmark map of forest carbon stocks in tropical regions across three continents, *Proceedings of the*
1238 *National Academy of Sciences*, **108** (24), 9899–9904.

1239 Sandberg, G., Ulander, L. M. H., Holmgren, J., Fransson, J. E. S., & Le Toan, T. (2011). L- and P-band
1240 backscatter intensity for biomass retrieval in hemiboreal forest, *Remote Sensing of the Environment*
1241 *115*, 2874-2886.

1242 Sandberg, G., Ulander, L. M. H., Wallerman, J., and Fransson, J.E.S. (2014). Measurements of forest
1243 biomass change using P-band SAR backscatter, *IEEE Trans. Geosci. Remote Sensing*, *52*(*10*), 6047-
1244 6061.

1245 Santoro, M., Beer, C., Cartus, O., Schmullius, C., Shvidenko, A., McCallum, I., et al. (2011). Retrieval
1246 of growing stock volume in boreal forest using hyper-temporal series of Envisat ASAR ScanSAR
1247 backscatter measurements. *Remote Sens. Environ.*, *115*(*2*), 490-507.

1248 Santoro, M., Cartus, O., Fransson, J. E. S., Shvidenko, A. , McCallum, I., Hall, R. J., et al. (2013).
1249 Estimates of forest growing stock volume for Sweden, Central Siberia and Québec using Envisat
1250 Advanced Synthetic Aperture Radar backscatter data. *Remote Sensing*, *5*(*9*), 4503-4532.

1251 Scharf, L. L. (1991). *Statistical signal processing: detection, estimation, and time series analysis.*
1252 *Boston: Addison–Wesley. ISBN 0-201-19038-9.*

1253 Schimel, D., Pavlick, R., Fisher, J.B., Asner, G.P., Saatchi, S. S., Townsend, P., et al. (2015). Observing
1254 terrestrial ecosystems and the carbon cycle from space, *Global Change Biology*, *21*, 1762-1776.

1255 Schmullius, C., Matejka, E., Pathe, C., Santoro, M., Cartus, O., Wiesmann, A., et al. (2017). *DUE*
1256 *GlobBiomass Final Report*, ESA-ESRIN Contract No. 4000113100/14/I_NB.

1257 Schlund, M., Scipal, K., and Quegan, S. (2018). Assessment of a power law relationship between P-
1258 band SAR backscatter and aboveground biomass and its implications for BIOMASS mission
1259 performance, *IEEE Jnl. Selected Topics in Applied Earth Observations and Remote Sensing*, *11*, 3538-
1260 3547, doi: 10.1109/JSTARS.2018.2866868.

1261 Skonieczny, C., Paillou, P., Bory, A., Bayon, G., Biscara, et al. (2015). African humid periods triggered
1262 the reactivation of a large river system in Western Sahara, *Nature Comm.*, Nov. 10th.

1263 Smallman, T. L., Exbrayat, J.-F., Mencuccini, M., Bloom, A., and Williams, M. (2017). Assimilation
1264 of repeated woody biomass observations constrains decadal ecosystem carbon cycle uncertainty in
1265 aggrading forests**,** *J. Geophys. Res. Biogeosciences, 122*, 528-545.

1266 Smith-Jonforsen, G., Folkesson, K., Hallberg, B., and Ulander, L. M. H. (2007). Effects of forest
1267 biomass and stand consolidation on P-band backscatter, *IEEE Geosci. Remote Sensing Letts*., *4*(*4*), 669-
1268 673.

1269 Soja, M. J., Sandberg, G., and Ulander, L. M. H. (2013). Regression-based retrieval of boreal forest
1270 biomass in sloping terrain using P-band SAR, *IEEE Trans. Geosci. Remote Sens.*, *51*(*5*), 2646-2665.

1271 Soja, M. J., Askne, J. I. H., and Ulander, L. M. H. (2017). Estimation of boreal forest properties from
1272 TanDEM-X data using inversion of the interferometric water cloud model, *IEEE Geosci. Remote*
1273 *Sensing Letts.*, *14*(*7*), 997-1001.

1274 Soja, M. J., d'Alessandro, M. M., Quegan, S., Tebaldini, S., and Ulander, L. M. H. (2018). Model-based
1275 estimation of tropical forest biomass from notch-filtered P-band SAR backscatter, *Proc. IEEE Int.*
1276 *Geosci. Remote Sensing Symp. (IGARSS 2018)*, Valencia.

1277 Tang, S. (2018). *Quantifying Differences in Forest Structures with Quantitative Structure Models from*
1278 *TLS Data*, MSc Thesis, University College London.

1279 Tebaldini, S., Mariotti d'Alessandro, M., Kim, J.-S., Papathanassiou, K. (2017). Ionosphere vertical
1280 profiling from BIOMASS multisquint InSAR, *Proc. IEEE Int. Geosci. Remote Sensing Symp. (IGARSS*
1281 *2017)*, Fort Worth (USA).

1282 Tebaldini S. and Rocca, F. (2012). Multibaseline polarimetric SAR tomography of a boreal forest at P-
1283 and L-bands, *IEEE Trans. Geosci. Remote Sens.*, *50*(*1*), 232-246.

1284 Thomas, S. C., and Martin, A. R. (2012). Carbon content of tree tissues: a synthesis, *Forests*, *3*, 332-
1285 352, doi:10.3390/f3020332.

1286 Thurner, M., Beer, C., Santoro, M., Carvalhais, N., Wutzler, T., Schepaschenko, D., et al. (2014).
1287 Carbon stock and density of northern boreal and temperate forests. *Global Ecology and Biogeography*,
1288 *23*(*3*), 297-310.

1289 Thurner, M., Beer, C., Ciais, P., Friend, A.D., Ito, A., et al. (2017). Evaluation of climate-related carbon
1290 turnover processes in global vegetation models for boreal and temperate forests, *Global Change*
1291 *Biology, 23*, 3076–3091.

1292 Treuhaft, R. N., Madsen, S. N., Moghaddam, M., and van Zyl, J. J. (1996). Vegetation characteristics
1293 and underlying topography from interferometric data, *Radio Sci*., *31*, 1449-1495.

1294 Truong-Loi, M.-L., Saatchi, S., and Jaruwatanadilok, S. (2015). Soil moisture estimation under tropical
1295 forests using UHF radar polarimetry, *IEEE Trans. Geosci. Remote Sens.*, *53*(*4*), 1718–1727.

1296 Ulander, L. M. H., Gustavsson, A., Flood, B., Murdin, D., Dubois-Fernandez, P., Dupuis, X., et al.
1297 (2011a). *BioSAR 2010: Technical Assistance for the Development of Airborne SAR and Geophysical*
1298 *Measurements during the BioSAR 2010 Experiment, Final Report*, ESA contract no.
1299 4000102285/10/NL/JA/ef.

1300 Ulander, L.M.H., Sandberg, G. & Soja, M.J. (2011b). Biomass retrieval algorithm based on P-band
1301 BioSAR experiments of boreal forest*, Proc. 2011 IEEE International Geosci. Remote Sensing Symp.*,
1302 Vancouver, Canada, 4245-4248.

1303 Ulander, L. M. H., Monteith, A. R., Soja, M. J., and Eriksson, L. E. B. (2018). Multiport vector network
1304 analyzer radar for tomographic forest scattering measurements, *IEEE Geosci. Remote Sensing Letters*,
1305 *15*(*12*), 1897 – 1901.
1306 UNFCCC (2016). *Key decisions relevant for reducing emissions from deforestation and forest*
1307 *degradation in developing countries (REDD+), Decision booklet REDD+*, UNFCCC secretariat,
1308 February 2016.
1309 Villard, L., and Le Toan, T. (2015). Relating P-band SAR intensity to biomass for tropical dense forests
1310 in hilly terrain: γ^0 or t^0?, *IEEE Jnl. Selected Topics in Applied Earth Observations and Remote Sensing*,
1311 *8*(*1*), 214-223.
1312 Warszawski, L., Frieler, K., Huber, V., Piontek, F., Serdeczny, O., and Schewe, J. (2014). The Inter-
1313 Sectoral Impact Model Intercomparison Project (ISI–MIP): Project framework, *PNAS*, *111*(*9*), 3228-
1314 3232; https://doi.org/10.1073/pnas.1312330110.
1315 Wessel, B., Huber, M., Wohlfart, C., Marschalk, U., Kosmann, D., Roth, A. (2018). Accuracy
1316 assessment of the global TanDEM-X Digital Elevation Model with GPS data, *ISPRS Jnl.*
1317 *Photogrammetry and Remote Sensing*, *139*, 171–182.
1318 Williams, M, Hill, T.C., and Ryan C.M. (2013). Using biomass distributions to determine probability
1319 and intensity of tropical forest disturbance, *Plant Ecology and Diversity*, *6*, 87-99.
1320 World Bank, *Wood-Based Biomass Energy Development for Sub-Saharan Africa: Issues and*
1321 *Approaches* (2011). The International Bank for Reconstruction and Development, The World Bank
1322 Group, Washington, D.C., U.S.A.
1323 Wright, P., Quegan, S., Wheadon, N., and Hall, D. (2003). Faraday rotation effects on L-band
1324 spaceborne SAR data, *IEEE Trans. Geosci. Remote Sensing*, *41*(*12*), 2735-2744.
1325
1326 **Figure captions**

Fig. 1. Global ecological regions of the world (FAO 2012) with the area affected by Space Objects Tracking Radar (SOTR) stations highlighted in yellow. Only land areas between 65° South and 85° North are represented (figure reproduced courtesy of Joao Carreiras).

Fig. 2. P-band backscatter at HV polarisation (γ^0_{HV}) over tropical and boreal forests against the biomass of *in situ* reference plots. Data from Paracou, French Guiana, were acquired by the SETHI SAR system in 2011 (Dubois-Fernandez et al., 2012), those from La Selva, Costa Rica, in 2004 by the AIRSAR system (Antonarakis et al., 2011) and those from Remningstorp, Sweden, by the E-SAR system in 2007 (Sandberg et al., 2011).

Fig. 3. Estimated AGB using the approach described in the text against AGB estimated from *in situ* and airborne laser scanning at the La Lopé site in Gabon during the AfriSAR campaign. The running average given by the blue line indicates only a small positive bias across the whole range of AGB. ROI denotes Region of Interest.

Fig. 4. Plot of HV backscatter intensity at height 30 m above the ground measured by tomography against *in situ* AGB in 1 ha plots at tropical forest sites investigated during the TropiSAR (Paracou and Nouragues) and AfriSAR (Lopé, Rabi, Mondah) campaigns.

Fig. 5. Forest height map obtained from inverting P-band Pol-InSAR data acquired over the Pongara National Park, Gabon, in the framework of the AfriSAR campaign in February 2017.

Fig. 6. (Top) Pair of repeat-pass PALSAR-2 images acquired on 8 August 2014 and 7 August 2015 displayed in Pauli image format (red = HH + VV; blue = HH - VV; green = 2HV) and slant range geometry. (Bottom left) Detection of change at 99% significance level; changed pixels are marked as black. (Bottom right) Image from 8 August 2014 with changed pixels marked as red.

Fig 7. Relative difference between modelled carbon turnover rates and turnover rates inferred from observations. 1.0 means modelled rate is 100% higher (from Thurner et al., 2017). Red boxes labelled b (boreal) and t (temperate) were analysed further in Thurner et al. (2017) to explain these discrepancies (figure reproduced courtesy of Martin Thurner).

Fig. 8. The relative reduction in the size of the 95% confidence interval of estimated vegetation carbon turnover times when using a prior value for biomass at each pixel compared to a run without a biomass

prior. Turnover times were estimated using the CARDAMOM system. The darker areas show where reduction in relative uncertainty is largest.

Figure 9. Left: SPOT image of the Ksar Ghilane oasis region in southern Tunisia: palaeo-channels are hidden by aeolian sand deposits. Middle: ALOS-2 L-band radar image, showing sub-surface features but blurred by the return from the superficial sand layer. Right: SETHI P-band radar image, clearly revealing sub-surface hydrological features.

Fig. 10. Coverage of ESA and NASA-ISRO satellite measurements of forest structure and above-ground biomass (AGB). The background shows the global coverage area of NISAR, which will be sensitive to AGB values < 100 t/ha (green and yellow). BIOMASS coverage includes the tropical belt, the temperate and boreal zones of Asia, and the southern hemisphere, while the GEDI Lidar will sample latitudes between ± 51.5°. These two sensors will cover the full range of forest AGB providing measurements where AGB >100 t/ha (red), so inaccessible to NISAR.